

# Geometric Awareness in Neural Fields for 3D Human Registration

Riccardo Marin<sup>1,2</sup> Enric Corona<sup>3</sup>  
Gerard Pons-Moll<sup>1,2,4</sup>

<sup>1</sup>University of Tübingen, Germany    <sup>2</sup>Tübingen AI Center, Germany    <sup>3</sup>Google Research

<sup>4</sup>Max Planck Institute for Informatics, Saarland Informatics Campus, Germany

{riccardo.marin, gerard.pons-moll}@uni-tuebingen.de, enriccorona@google.com



Figure 1. Our method (INLoVD) provides reliable point cloud human registrations in disparate conditions. Trained on AMASS, a large MoCap dataset for SMPL, we test INLoVD on more than 5K shapes from more than 10 data sources. INLoVD generalizes to real scans, partial and cluttered point clouds, clothed humans, loose garments, identities out of distribution, and challenging poses. Meshes are depicted for visualization purposes and are not used by our method.

## Abstract

Aligning a template to 3D human point clouds is a long-standing problem crucial for tasks like animation, reconstruction, and enabling supervised learning pipelines. Recent data-driven methods leverage predicted surface correspondences; however, they are not robust to varied poses or distributions. In contrast, industrial solutions often rely on expensive manual annotations or multi-view capturing systems. Recently, neural fields have shown promising results, but their purely data-driven nature lacks geometric awareness, often resulting in a trivial misalignment of the template registration. In this work, we propose two solu-

tions: *LoVD*, a novel neural field model that predicts the direction towards the localized SMPL vertices on the target surface; and *INT*, the first self-supervised task dedicated to neural fields that, at test time, refines the backbone, exploiting the target geometry. We combine them into INLoVD, a robust 3D Human body registration pipeline trained on a large MoCap dataset. INLoVD is efficient (takes less than a minute), solidly achieves the state of the art over public benchmarks, and provides unprecedented generalization on out-of-distribution data. We will release code and checkpoints in [url](#).

## 1. Introduction

Registration of 3D surfaces is a crucial area of research in Computer Vision, playing a vital role in analyzing shape collections, pattern discovery, and statistical model training. Among all the 3D surfaces, human models are of particular importance. It is worth noting that human registration has enabled the development of today’s standard human parametric model (SMPL from [44]) and also facilitates several downstream tasks such as animation, virtual try-on, and is the driving force behind virtual and mixed reality.

However, human registration presents several challenges. Articulations can take various configurations, leading to blind spots and geometry gluing (for instance, due to self-contact), even when hundreds of cameras are involved. Fine-grained details characterize human identities, and their reconstruction is essential to represent human diversity. Finally, the acquisition process is noisy, especially when low-resource settings (like Kinect depth scans) or even customer-level devices (such as applying NeRF-based systems like [45] to smartphone RGB videos) are used.

Scholars approach shape registration intrinsically or extrinsically. Intrinsic approaches, favored by Computer Graphics ([49, 53, 60, 70]), obtain pair-wise correspondences between shapes, restricting solutions to the object’s surfaces and guaranteeing invariance to rigid deformations. These methods are often impractical for real data, as clutter and noise often ruin their theoretical premises. Extrinsic registration pipelines, popular in Computer Vision research ([8, 41, 42, 66, 81]), rely on templates as regularizers. However, these pipelines require expert annotators, multi-camera views, and priors for specific settings, which makes them inapplicable in many use cases. The final template deformation may fall apart from the target surface even with robust learned priors. A common practice to refine template alignment is to iterate between Euclidean correspondence and registration until convergence, as done in the popular Iterative Closest Point (ICP) of [5] and its variants (e.g., [39]). However, the pairing step is sensitive to initialization and noise, leading often to local minima.

Recently, a promising direction has been developed on registration methods based on Neural Fields (NF) (e.g., LVD, [20]). The deformation field is trained to predict to point from a query point in  $\mathbb{R}^3$  toward template registration vertices. However, such a rich representation is purely data-driven and does not incorporate any geometrical sense of the target shape. Instead, our inspiration is to enrich the learned prior with geometric awareness. First, we propose **LoVD**, a Localized Vertex Descent that relies on a spectral segmentation of the template to define many localized query heads, each dedicated to a specific geometric region. This template segmentation (which runs only once before starting the training) is automatic, theoretically sound, and flexible in defining the number of desired segments. Then,

we propose the Iterative Neural Tuning **INT**, the first self-supervised task that, at inference time, enhances the NF geometric awareness. Concretely, INT queries the NF directly on *the vertices of the target shape* at inference time. For each point on the target, we pair it with the template vertex *corresponding to the predicted offset with the minimum norm*, i.e., the closest template point indicated by the NF. Secondly, we sum the retrieved smallest offsets for all the target points, and we use this as a loss to *fine-tune the NF by backpropagation*. This simple procedure is based on ICP principles: NF deformation suggests a correspondence, which we use to update the deformation. INT is the first refinement specifically designed for NF, takes a few seconds, and improves the backbone registration up to 30%. Furthermore, INT enables an unprecedented generalization out of distribution, including real scans, identities, poses, garments, and even noise from Kinect fusion and partial scans.

Finally, we integrate LoVD and INT in **INLoVD**, a robust and efficient registration pipeline. Using a *single network* trained on the large MoCap dataset from [47] (AMASS), we provide a ready-to-go method tested on more than 5k shapes and 10 different data sources; Figure 1 shows a subset of these, and colors encode the correspondence provided by our registration. We stress it with an unprecedented variety of poses, identities, and real-world challenges far from training distribution (e.g., garments, noise point clouds, clutter, partiality). We improve state-of-the-art benchmarks for human body registration for methods trained on similar assumptions and surpassing approaches with stronger priors. We will release our code and weights of the network, providing a tool that, out of the box, offers robust human registration in *less than a minute*. In summary, our contributions are:

1. **LOVD**: A novel localized neural field where network architecture is designed following a geometrical spectral segmentation of the template; this variant provides a domain-agnostic method that improves the NF performance.
2. **INT**: The first self-supervised fine-tuning procedure to improve geometric understanding of an NF at inference time, which largely improves registration performance and opens to unprecedented generalization
3. **INLoVD Registration Pipeline**: We integrate LoVD and INT in a full human registration pipeline trained on a large MoCap dataset, advancing state of the art on public benchmarks and challenging real cases.
4. **Code and data release**: We release the code for processing, training, and evaluation, together with network weights; we provide researchers with a way-to-go tool for 3D Human registration that works in many different contexts out of the box.

## 2. Related Works

Shape correspondence has a vast literature, and while we list the works that mainly inspired us, we point to [22] for a recent and extensive survey.

**Shape matching.** A straightforward idea to solve the correspondence problem is to compute a space for the vertices of the shapes where they are naturally aligned (canonical embedding). Classical approaches in this category are the multi-dimensional scaling from [11], and descriptors proposed by [70] (HKS), [3] (WKS), and [67] (SHOT). Their dependence on input geometry does not generalize well in the presence of noise. Recently, [50] proposes a deep learning variation as a baseline. Still, such a unified representation is challenging to learn for non-rigid shapes. Works like [15, 16, 36] propose canonicalizing human shapes by inferring a common skeleton from external views, but they suffer from occlusions. A recent trend ([32, 35, 50]) is to learn a representation where a linear transformation can align shapes. These methods rely on pseudo-inverse computation at training time, which hardly scales and produces numerical instability. Their inspiration can be found in the Functional Maps framework of [60], an elegant and theoretically grounded formulation which opened to a set of regularization and variations ([51, 59, 62]), as well as refinements ([33, 53]). Mainly based on the eigenfunctions of the Laplace-Beltrami Operator, its applications are limited to clean meshes and unrealistic partialities ([21, 54, 64]).

**Shape Registrations.** A widely explored approach to recover the correspondence is solving the alignment problem by registering the pair of shapes in  $\mathcal{R}^3$ . A fundamental algorithm for the rigid case is ICP from [5], which aligns two shapes by iterating between the deformation and the correspondence. The simplicity of ICP made it broadly used, but its sensitivity to noise and initialization may limit the convergence toward a local minimum. Countless variations have been proposed; for example, [10] and [18] address the sparsity and noise, respectively, but they still require careful design choices. Interestingly, [75] and [78] propose a deep learning approach to provide a more reliable correspondence. Still, they are both limited to rigid deformation. Instead, iterative algorithms to recover non-rigid deformation like [39] often rely on optimizations that trade some rigidity for a more expressive deformation. The Coherent Point Drift proposed in [57] exploits a probabilistic formulation, which got a new life following probabilistic shapes representations ([30, 31]). Deep learning follow-ups from [40] and [74] tried to learn the deformation from data. Their learning of point-wise features assumes limited non-rigid deformations and the absence of clutter. Finally, templates provide strong regularization ([29, 82]), and this direction has been widely investigated ([6, 28, 71, 72]) — but the registration often falls far from the target surface.

**3D Human registration.** The classic work of [8] uses

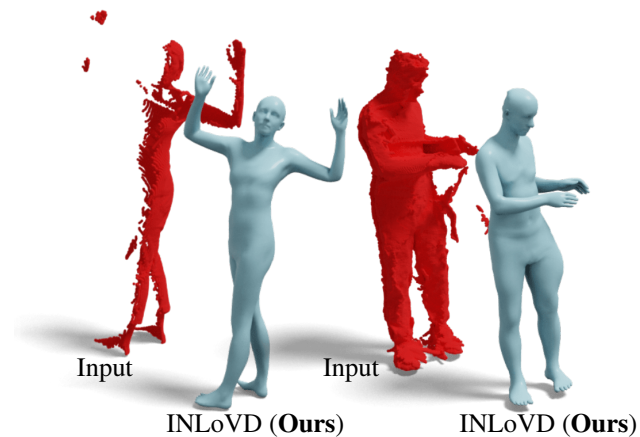


Figure 2. Input and results of our method on some challenging shapes from Cape [46] and BEHAVE [7].

expert feedback and controlled setups to lead 3D registration. More flexible, the stitched puppet of [80] automatically solves piece-wise optimization of the local body parts, but gluing them leads to major artifacts. [49] introduced FARM, an automatic method with 3D landmark detection, which [48] extended for high resolution. Both rely on the Functional Map of [60] and struggle with non-watertight meshes. With the advent of learning, the seminal work of [28] proposed a simple yet effective autoencoder architecture. Its global nature motivated follow-up works of [23] and [72] to learn local and attention-based relations, but both suffer from clutter. [36] propose Deep virtual markers (DVM), using synthetic multi-view depth representation. DVM requires a demanding manually annotated training set and suffers from occlusions and self-contact. [25] propose to solve complex poses by enforcing rotation invariance of local parts. Such design assumes clean data and does not generalize to real-world challenges like garments, noise, or other artifacts of local geometry without an ad-hoc training set. Instead of directly predicting the position of the points, [71] output offsets. While similar in principle to predicting space positions, this output representation is richer and predisposed to regularization. Such regularizations are expensive, limiting applicability to small training distributions. [20] recently proposed Learned Vertex Descent (LVD), which instead regularizes the training using an even richer representation for the template deformation. Their idea is to train a network that, given an input shape, produces an NF defined all over  $\mathbb{R}^3$ . Querying the NF to a 3D point predicts the ordered offsets toward all the registered template vertices. Supervising the training on every 3D location toward all the template vertices produces a robust data-driven prior that benefits from large-scale datasets. However, LVD is also highly dependent on the training distribution, and often errors cannot be recovered even with Chamfer distance optimization.

# Neural Fields

Neural Fields lack a sense of geometry → × Bounded by the training distribution × Cannot recover from trivial errors

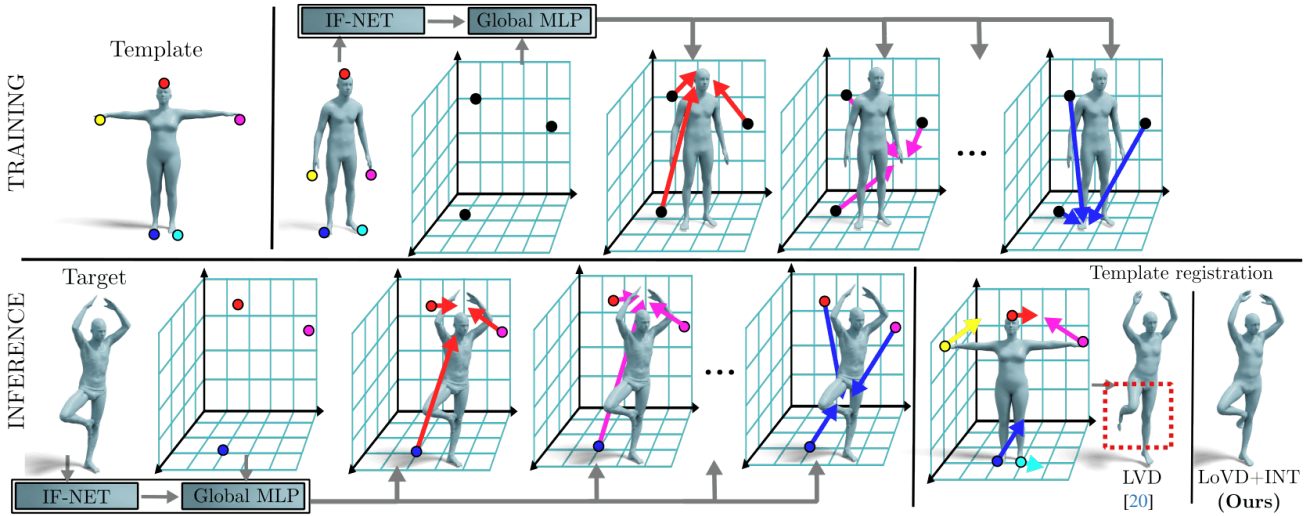


Figure 3. NF for human registration. During training (top), the network learns to predict, for every query point in space (black dots), the ordered ground-truth offsets toward the template vertices (colored dots). At inference time (bottom), given a target shape, the template vertices locations are queried. The template vertices are then aligned by applying the predicted ordered offsets to them. The lack of geometrical awareness often produces trivial misalignment. Our method address this problem.

## 3. Background

### 3.1. Point Cloud Registration

3D Point cloud registration is the process of spatially aligning a template with an unsorted target point cloud while respecting its semantics. Given a template with ordered points  $\mathbf{X} \in \mathbb{R}^{m \times 3}$  and an unsorted target point cloud  $\mathbf{Y} \in \mathbb{R}^{n \times 3}$ , the goal is to recover a deformation  $F : \mathbf{X} \rightarrow \hat{\mathbf{X}} \in \mathbb{R}^{m \times 3}$  such that  $\hat{\mathbf{X}}$  aligns with  $\Pi(\mathbf{Y})$  under a permutation  $\Pi : \mathbf{Y} \rightarrow \hat{\mathbf{Y}} \in \mathbf{Y}^m$ , which encodes the correspondence:

$$\|F(\mathbf{X}) - \Pi(\mathbf{Y})\|_F = 0. \quad (1)$$

However, the real case is more complex as the correspondence  $\Pi$  is not always bijective due to different numbers of points, partial views, noise, and clutter. As a result, often Equation 1 does not have a ground-truth solution and is solved by optimization. Figure 2 shows examples of partial and cluttered input (red point clouds), as well as the output of our method (grey meshes).

**Iterative registration** Among the possible optimizations to solve Equation 1, a popular solution is to iterate between the correspondence and the deformation such that they refine each other till convergence. A famous seminal example is the Iterative Closest Point (ICP) algorithm from [4]. Starting from an initial configuration of the two shapes (*i.e.*,  $\tilde{F}(\mathbf{X}) = \mathbf{X}$ ), ICP recovers the correspondence using an Euclidean nearest-neighbor pairing:

$$\tilde{\Pi} = \arg \min_{\Pi} \|\tilde{F}(\mathbf{X}) - \Pi(\mathbf{Y})\|_2^2. \quad (2)$$

Next, ICP updates  $\tilde{F}$  by minimizing the point-to-point distance with a least-squares objective:

$$\tilde{F} = \arg \min_F \sum_{i=1}^m \|F(\mathbf{x}_i) - \tilde{\Pi}(\mathbf{Y})_i\|_2^2. \quad (3)$$

These two steps are iterated multiple times until convergence. As a main limitation, the correspondence step is sensitive to noise. The Euclidean nearest-neighbor pairing is undesirable both for computational and stability reasons and requires ad-hoc mitigation strategies in the presence of outliers ([27, 55, 77]). ICP converges at a global minimum only when the shapes are already roughly aligned.

**Neural Fields for registration** Neural Fields (NF) have been proven to be a powerful representation of 3D geometry, which parametrizes a quantity defined all over a domain coordinates (a field) using a neural network [76]. [20] firstly propose their use for solving the registration problem, calling this procedure Learned Vertex Descent (LVD). The idea is to train a neural network  $F^\theta : \mathbb{R}^3 \rightarrow \mathbb{R}^{n \times 3}$  that, for any point in  $\mathbb{R}^3$ , outputs the ordered offsets toward the  $n$  vertices of the desired deformed template  $\hat{\mathbf{X}}$  (Figure 3, top). At inference time, the network produces the NF for a target shape (Figure 3, bottom left). The location  $\hat{\mathbf{x}}_i$  of the  $i$ -th registered template vertex is obtained by querying the NF on  $\mathbf{x}_i$  and following the  $i$ -th predicted offset  $F^\theta(\mathbf{x}_i)_i$  (Figure 3, bottom right):

$$\hat{\mathbf{x}}_i = \mathbf{x}_i + F^\theta(\mathbf{x}_i)_i \quad (4)$$

**NF Limitations.** NF prediction is based on the data prior given by the training set and does not incorporate any geometrical awareness of the class of shapes or consider the target geometry. Hence, NF are bounded by their training distribution; considering the variety of human identities and poses (further complicated by clutter, *e.g.*, garments), it is common for NF to miss the target (Figure 3, bottom right).

## 4. Method

**Overview of INLoVD.** Our 3D Human registration pipeline starts from a 3D point cloud; all the mesh depicted in this paper is just for visualization purposes and are not used. The input is passed to a localized backbone network with multiple heads that obtain NF for local parts of the shape. Before letting the NF converge, we refine it using INT, a self-supervised task that iteratively improves the backbone. Then, we use the updated NF to register the template to the input point cloud. The registration output by the network is further refined by Chamfer optimization and, if high-frequency details are required, also by vertex displacement.

### 4.1. Local Vertex Descent (LoVD).

We propose a novel variant of LVD that employs multiple MLPs heads, each specialized in predicting offsets only for vertices in a local template region. In choosing how to specialize the  $m$  local MLPs, a natural choice for humans would be relying on the 24 skinning weights distribution of SMPL, which has significant drawbacks. It requires setting thresholds and testing different numbers of segments (*e.g.*, 10 or 16) and requires manual design. Also, this partition would be redundant with the prior given by the training data. We decided instead to rely on spectral clustering as described in [43]. This algorithm requires computing the Laplace-Beltrami Operator for the surface, collecting its  $m$  eigenvectors associated with the  $m$  smallest eigenvalues, and using them as features for K-Means clustering, using  $m$  clusters. We use the Laplace-Beltrami Operator discretization of [69]. We discovered that having  $m = 16$  local MLPs associated with as many segments yields the best results (please check the Sup.Mat. for an ablation). This segmentation is performed only once, on the template, before the training starts, and affects only the network design. We depict our Localized Vertex descent (LoVD) and the template segmentation on the left of Figure 4.

### 4.2. Iterative Neural Tuning (INT)

NF defines a deformation that can be queried over the entire  $\mathbb{R}^3$ , also so on the target shape. Template registration should align with the target, so we expect that queries of the NF on the target vertices produce one or more offsets with norms close to 0. Our iterative self-supervised task is to promote this desirable property. Given a target shape, we iterate two steps. First, we *solve for the correspondence*:

we sample points  $\mathbf{y}_k$  over the target shape and use them to query the NF. We pair every query point with the template vertex that has the predicted offset with the minimum norm in that point:

$$\tilde{i}_k = \arg \min_i \|F^{\tilde{\theta}}(\mathbf{y}_k)_i\|_2^2, \quad (5)$$

which replaces the Euclidean arg min of Equation 2 with one suggested by the network data prior.

Secondly, we *solve for the registration*: we sum the minimum offsets  $F^{\theta}(\mathbf{y}_k)_{\tilde{i}_k}$  for all the query points  $\mathbf{y}_k$ , and we backpropagate this amount to update the NF parameters:

$$\tilde{\theta} = \arg \min_{\theta} \sum_{k=1}^n \|F^{\theta}(\mathbf{y}_k)_{\tilde{i}_k}\|_2^2. \quad (6)$$

Namely, we refine the field such that the deformation converges toward the estimated correspondence (*i.e.*, it predicts a 0 offset for the associated template vertex). Iterating these two steps refines the backbone network. We stress that our Iterative Neural Tuning (INT) is a self-supervised fine-tuning performed *at inference time*, does not require data or supervision, and is the first of its kind for neural fields.

### 4.3. NF Geometric Aware Registration (INLoVD)

**Input.** Given an input point cloud, we only assume a rough estimation of the Y-axis, while the points can be rotated in any other direction. Such assumption is standard in human body registration pipelines like the ones from [28] and [72], and can be easily approximated, for example, by computing robust landmarks for the shapes as in [49].

**INLoVD and template fitting.** Given a target point cloud, we use LoVD to obtain the NF, and we fine-tune with INT by iterating between Equation 5 and Equation 6. We update the network weights 20 times with a learning rate of  $1e-5$ . The whole procedure takes around 3 seconds. Then, we use the NF to move the points of the template and, as in [20], we fit a SMPL model to the prediction, using the same identity and pose prior penalizations [61].

**Refinement.** A common practice is to refine the template parameters with a Chamfer distance optimization. When we assume bijectivity between the template and target, we use the bidirectional one; otherwise, we rely on a single direction as in [6]. Finally, in cases where a high resolution is required, following the spirit of [48], we use SMPL+D to catch the finer details of the target, regularizing the displacements with a Laplacian energy [26]. Further technical details of the whole pipeline are in Sup.Mat.

**Naming Methods.** We will use *LoVD* for results obtained by fitting SMPL to the LoVD prediction, without further tunings; *+INT* when we apply our iterative task before NF convergence; *LoVD+INT* when we combine the LoVD and INT; *INLoVD* when LoVD+INT result is further refined. All results with these names are part of our contribution.

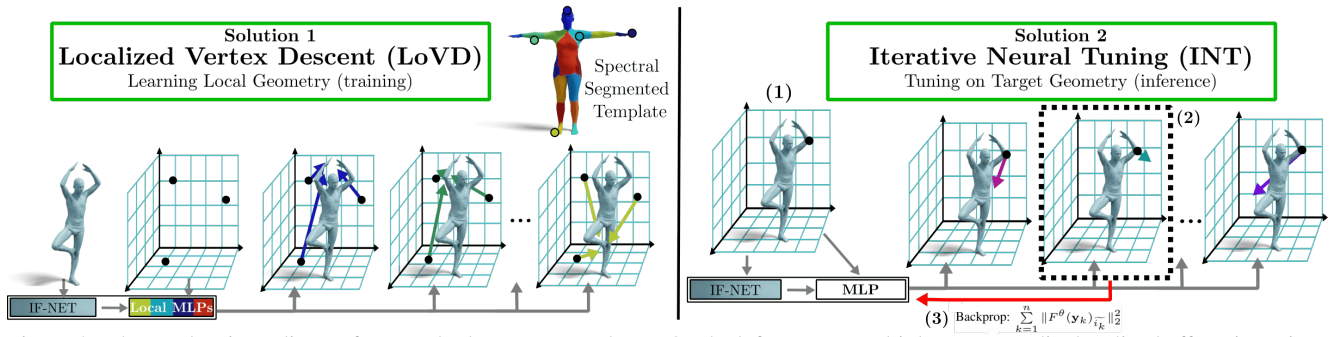


Figure 4. The two key ingredients of our method are LoVD and INT. On the left, LoVD. Multiple MLPs predict localized offsets in regions defined by spectral clustering of the template. On the right, INT. (1): At inference time, we query points on the target surface; (2): For each query point, we select the offset with the minimum norm; (3): The sum of the retrieved norms for all the vertices is used to fine-tune the backbone NF. INT is backbone agnostic, and applies to both global and local MLPs configurations.

## 5. Results

**Remark.** All shown results are obtained starting from *the same network weights*. The quantitative and qualitative experiments stress our method on the FAUST ([8]) and SHREC19 ([52]) challenges; this latter collects shapes from 10 different datasets. We also consider partial point clouds from CAPE ([46]) and Kinect ones from BEHAVE ([7]), NeRF-based 3D human reconstructions from LumaAI [45] and cases significantly out of distribution from the [68] Scan the World Project and TOSCA ([12]). We report results for challenging poses from SCAPE ([1]), clothed humans from Twindom ([73]), and RenderPeople ([63]), and output of acquisition pipeline as Dynamic-Faust ([9]) and the recent HuMMan dataset ([14]). We are unaware of any other method that provides an extensive evaluation and generalization, such as the one shown here and in the Sup.Mat..

**Template.** We consider the human SMPL model sampled at 690 vertices as a template; hence, our NF will provide  $690 \times 3$  values for each point. This subsample speeds training and inference up while we retain enough information to fit a complete SMPL model.

**Data.** To train the NF, we leverage the large MoCap AMASS dataset of [47], adopting the official splits. The train set comprises roughly 120k SMPL+H [65] shapes animated with motion-captured sequences. We train for 10 epochs ( $\sim 157k$  steps). We report implementation details in Sup.Mat.. We rely on the FAUST challenge’s training set for validation and ablations. We consider as input both the scans (**Faust<sub>S</sub>**,  $\sim 170K$ - $200K$  vertices, noisy) and the ground-truth registrations (**Faust<sub>R</sub>**, 6890 vertices, clean).

**Baselines.** We compare against methods using the same feature extractor and training set. First, we consider the original LVD formulation (**LVD**) as described in the previous section. We also propose *OneShot*, a baseline that predicts offsets toward the registered template vertices for every point in  $\mathbb{R}^3$  in a single pass. We reimplemented the Universal embedding baseline proposed by [50], which learns a high-dimensional embedding where shapes are naturally aligned, and so the correspondence is obtained by Euclidean

	FAUST <sub>R</sub>	FAUST <sub>S</sub>
OneShot	4.45	3.34
OneShot + INT (Ours)	3.64	3.15
LVD	4.78	3.54
LVD + INT (Ours)	3.40	2.81
LoVD (Ours)	4.35	3.11
LoVD + INT (Ours)	2.97	2.55

Table 1. NF comparisons. We show that our LoVD is the best NF out of the box, and our INT procedure improves all the backbones.

nearest neighbor. We consider a 60 dimensional embedding (**Uni-60**) as proposed by [50], and also a 2070 one (**Uni-2070**) to have similar output dimensions of our method (690 offset of 3 dimensions).

**Metrics.** For the test on the FAUST training, FAUST challenge, and BEHAVE, the error is measured in centimeters as the Euclidean distance from the predicted point position and the ground truth. On SHREC19, the error is the normalized geodesic distance [37].

**Computational timing.** We conduct our experiments on a computer equipped with a 12-core CPU AMD Ryzen 9 5900X, an NVIDIA GeForce RTX 3080 Ti GPU, and RAM 64GB. The entire INT requires 3–4 seconds; INLoVD registration for a single shape is around 60 seconds.

### 5.1. Validation

**LoVD.** In Table 1, we compare our new localized neural field against other NF networks. Even before our INT procedure, LoVD is the NF that works the best out of the box. All the NF use the same features and training dataset, proving the effectiveness of our design choice. We include an ablation for different amounts of segments in Sup.Mat..

**INT.** In Table 1, we show the effect of the INT procedure on different NF. INT solidly improves all the backbones, showing generalization without requiring data or supervision. We also report its application on a pre-trained network for a different domain (*i.e.*, hand registration) in Sup.Mat..

**LoVD+INT.** The combination of our two ingredients improves on the two datasets **30%** and **23%** w.r.t. the best available NF (OneShot). This result further proves the high impact of making the NF geometric aware.

**INLoVD.** Table 2 reports the comparison with methods

	FAUST <sub>R</sub>	FAUST <sub>S</sub>
Uni-60 ([50])	3.52	2.66
Uni-2070 ([50])	3.49	2.62
LVD ([20])	4.78	3.54
LVD+Chamfer [20]	2.15	1.93
<b>INLoVD (Ours)</b>	<b>1.76</b>	<b>1.85</b>

Table 2. Comparison with complete methods for human registration. They all use the same data and feature extractors.

	BEHAVE	Input	GT	LoVD	LoVD+INT
LoVD	6.78				
LoVD+INT	<b>5.69</b>				

Table 3. INT robustness to noise. On the left, quantitative registration error on 3320 frames of [7]; INT improves on average 17.6% over the backbone and improves results on 80% of the frames. On the right is a qualitative result.

	INTRA	INTER
Loopreg ([6])	1.35	2.66
Elementary ([23])	1.74	2.58
UD2E-Net ([17])	1.51	3.09
<b>INLoVD (Ours)</b>	<b>1.06</b>	<b>2.26</b>
DVM (multi-view) <sup>†</sup> ([36])	1.19	2.37

<sup>†</sup>: Has seen FAUST training set

Table 4. Results from the public leaderboard on INTRA- and INTER-subject FAUST challenges.

trained on the same dataset and the same feature extractor. We notice that the Uni baselines are a challenging competitor, able to surpass recent methods ([20]). LVD+Chamfer differs from INLoVD for the backbone (LoVD) and the use of INT. Our improvement (around **20%** on FAUST<sub>R</sub>) highlights how our geometrical awareness provides a better initialization to Chamfer refinement.

**INT Generalization and Robustness.** INT updates the network by randomly sampling the target input point cloud. Since this procedure is self-supervised, we wonder how sensitive it is to outliers. Hence, we test INT on the BEHAVE dataset proposed in [7]. It includes point clouds from Kinect multi-view depths and presents significant noise (*e.g.*, clutter, missing human parts due to occlusions). We uniformly sample 3320 frames from the sequences, register the fused depth point cloud, and compare the error with the provided ground truth registrations. Results are displayed in Figure 2, Table 3, and many others are reported in Sup.Mat.. INT enhances the backbone by around **17.6%**, and **improves on 80% of the frames**; it enables robust generalization on clutter and partiality without having seen it at training time, which is often mandatory for other methods ([2], [34]).

## 5.2. 3D Human Body Registration

**FAUST Challenge.** We test our pipeline on real data from the two FAUST challenges<sup>1</sup> from [8]. The scans are of 10 subjects in 20 poses (200 samples), with missing regions

<sup>1</sup><https://faust-leaderboard.is.tuebingen.mpg.de/leaderboard>

	SHREC19
LIE ([50])	15.1
GeoFMAP ([24])	11.2
CorrNet3D ([79])	9.6
3DCoded ([28])	10.3
Transmatch ([72])	6.1
ReduceBasis ([71])	4.8
<b>INLoVD (Ours)</b>	<b>2.27</b>

Table 5. Results on SHREC19 challenge [52]. We improve the state of the art by 53%

and clutter due to the noise in the acquisition process. Table 4 reports the error results from the leaderboard. We list the methods with similar assumptions to ours in the upper part of the table, on which we achieve an improvement of **20% and 12%** on the INTRA-subject and INTER-subject challenges, respectively. We also outperform DVM [36], which requires a manually artist-annotated dataset for training, the render of 72 synthetic views of the target for inference, and *have seen FAUST shapes at training time*, while we do not. We report qualitative results in Sup.Mat..

**SHREC19.** We test our method’s generalization on the recent and challenging dataset SHREC19 [52]. This database is a collection of 44 shapes from different datasets, facing various challenges: holes, out-of-distribution identities, disconnected components (*e.g.* earrings), clutter, and different densities (shapes have from 5k to 200k vertices). The ground truth on this data is provided by a robust registration method that exploits surface information. In Table 5, we report our results and the leaderboard from [71]. Our method significantly outperforms previous state-of-the-art and improves **53%**. Qualitative results are in Sup.Mat.

## 5.3. Applications

**Unifying data sources.** There are many different procedures to acquire 3D Human models. Our registration method based on point cloud geometry with no further assumption on the input source (*e.g.*, availability of RGB, subject orientation) can provide a standard for research, industry, and customer-level applications. In Figure 5, we show registration results on four datasets obtained with respectively with Kinects, a 4D scanner, a multi-view RGB-D dome, and a static body scanner. In Figure 6, we register a geometry extracted by a NeRFs [56], trained on a mobile phone video and using LumaAI website [45].

**Automatic Rigging of noise acquisitions.** Reliable registrations can be used to transfer information between aligned assets, like rigging. In Figure 6, we obtain an animatable avatar from a noise NeRF acquisition and apply a MoCap animation sequence. The entire procedure, from data acquisition to animation, can be automatized, opening vast possibilities for content creation applications.

## 6. Conclusions

We introduced two techniques to provide geometric awareness into NF: LoVD, a backbone with localized MLPs that



Figure 5. Results on shapes acquired with Kinects (BEHAVE), a 4D Scanner (DFAUST), a Multi-view RGB-D dome (HuMMAN), and a static full-body scanner (Twindom). Our method works out of the box in multiple applicative contexts. Further qualitative examples are provided in Sup.Mat..

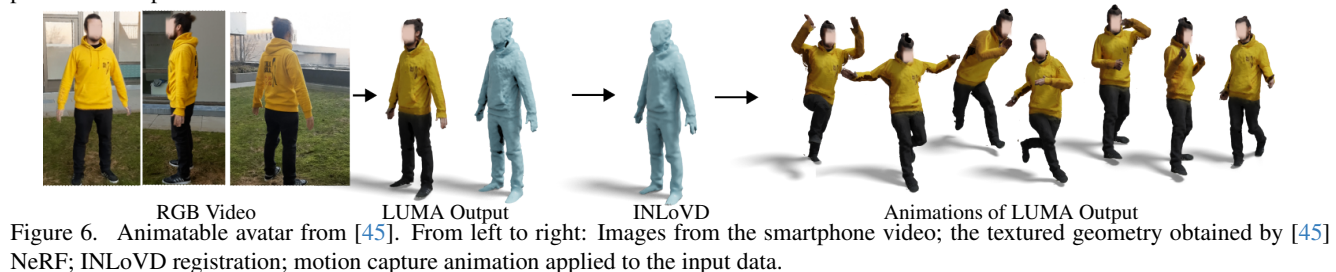


Figure 6. Animatable avatar from [45]. From left to right: Images from the smartphone video; the textured geometry obtained by [45] NeRF; INLoVD registration; motion capture animation applied to the input data.

focus on regions defined by spectral segmentation, and INT, an inference time self-supervised task that, in seconds, improves the accuracy and generalization of the backbone. Their union produces a performance boost which can reach 30%. We integrate them in INLoVD, a registration pipeline for 3D Humans trained on a large MoCap dataset. Our method achieves state of the art in multiple benchmarks, showing robustness to noise and incomplete point clouds, clothing, poses, and all *using the same network weights*. In Supplementary Material, we discuss failure modes and exciting directions for future works. Our method and the release of code and network weights will simplify current 3D registration pipelines, providing a valuable tool for several Computer Vision tasks, users, and researchers.

**Acknowledgments:** Special thanks to RVH team members; their feedback helped improve the manuscript. The project was made possible by funding from the Carl Zeiss Foundation. This work is supported by the Deutsche Forschungsgemeinschaft (DFG, German Research Foundation) - 409792180 (Emmy Noether Programme, project: Real Virtual Humans), German Federal Ministry of Education and Research (BMBF): Tübingen AI Center, FKZ: 01IS18039A. Gerard Pons-Moll is a member of the Machine Learning Cluster of Excellence, EXC number 2064/1 - Project number 390727645. Riccardo Marin has been supported by the European Union’s Horizon 2020 research and innovation program under the Marie Skłodowska-Curie grant agreement No 101109330.

## References

- [1] Dragomir Anguelov, Praveen Srinivasan, Daphne Koller, Sebastian Thrun, Jim Rodgers, and James Davis. Scape: shape completion and animation of people. In *ACM SIGGRAPH 2005 Papers*, 2005. 6
- [2] Souhaib Attaiki, Gautam Pai, and Maks Ovsjanikov. Dpfm: Deep partial functional maps. In *2021 International Conference on 3D Vision (3DV)*, pages 175–185. IEEE, 2021. 7
- [3] Mathieu Aubry, Ulrich Schlickewei, and Daniel Cremers. The wave kernel signature: A quantum mechanical approach to shape analysis. In *2011 IEEE international conference on computer vision workshops (ICCV workshops)*, pages 1626–1633. IEEE, 2011. 3
- [4] Paul J Besl and Neil D McKay. Method for registration of 3-d shapes. In *Sensor fusion IV: control paradigms and data structures*, pages 586–606. Spie, 1992. 4
- [5] Paul J Besl and Neil D McKay. Method for registration of 3-d shapes. In *Sensor fusion IV: control paradigms and data structures*, pages 586–606. Spie, 1992. 2, 3
- [6] Bharat Lal Bhatnagar, Cristian Sminchisescu, Christian Theobalt, and Gerard Pons-Moll. Loopreg: Self-supervised learning of implicit surface correspondences, pose and shape for 3d human mesh registration. *Advances in Neural Information Processing Systems*, 33:12909–12922, 2020. 3, 5, 7
- [7] Bharat Lal Bhatnagar, Xianghui Xie, Ilya A Petrov, Cristian Sminchisescu, Christian Theobalt, and Gerard Pons-Moll. Behave: Dataset and method for tracking human object interactions. In *Proceedings of the IEEE/CVF Conference on Computer Vision and Pattern Recognition*, pages 15935–15946, 2022. 3, 6, 7, 8
- [8] Federica Bogo, Javier Romero, Matthew Loper, and Michael J Black. Faust: Dataset and evaluation for 3d mesh registration. In *Proceedings of the IEEE conference on computer vision and pattern recognition*, pages 3794–3801, 2014. 2, 3, 6, 7, 20
- [9] Federica Bogo, Javier Romero, Gerard Pons-Moll, and Michael J Black. Dynamic faust: Registering human bodies in motion. In *Proceedings of the IEEE conference on computer vision and pattern recognition*, pages 6233–6242, 2017. 6, 8, 14, 20
- [10] Sofien Bouaziz, Andrea Tagliasacchi, and Mark Pauly. Sparse iterative closest point. In *Computer graphics forum*. Wiley Online Library, 2013. 3
- [11] Alexander M Bronstein, Michael M Bronstein, and Ron Kimmel. Generalized multidimensional scaling: a framework for isometry-invariant partial surface matching. *Proceedings of the National Academy of Sciences*, 103(5):1168–1172, 2006. 3
- [12] Alexander M Bronstein, Michael M Bronstein, and Ron Kimmel. *Numerical geometry of non-rigid shapes*. Springer Science & Business Media, 2008. 6, 17
- [13] Andrei Burov, Matthias Nießner, and Justus Thies. Dynamic neural radiance fields for monocular 4d facial avatar reconstruction, 2021. 17
- [14] Zhongang Cai, Daxuan Ren, Ailing Zeng, Zhengyu Lin, Tao Yu, Wenjia Wang, Xiangyu Fan, Yang Gao, Yifan Yu, Liang Pan, et al. Humman: Multi-modal 4d human dataset for versatile sensing and modeling. In *Computer Vision—ECCV 2022: 17th European Conference, Tel Aviv, Israel, October 23–27, 2022, Proceedings, Part VII*, pages 557–577. Springer, 2022. 6, 8, 20
- [15] Zhe Cao, Tomas Simon, Shih-En Wei, and Yaser Sheikh. Realtime multi-person 2d pose estimation using part affinity fields. In *CVPR*, 2017. 3
- [16] Z. Cao, G. Hidalgo Martinez, T. Simon, S. Wei, and Y. A. Sheikh. Openpose: Realtime multi-person 2d pose estimation using part affinity fields. *IEEE Transactions on Pattern Analysis and Machine Intelligence*, 2019. 3
- [17] Ronghan Chen, Yang Cong, and Jiahua Dong. Unsupervised dense deformation embedding network for template-free shape correspondence. In *Proceedings of the IEEE/CVF International Conference on Computer Vision (ICCV)*, pages 8361–8370, 2021. 7
- [18] Dmitry Chetverikov, Dmitry Svirko, Dmitry Stepanov, and Pavel Krsek. The trimmed iterative closest point algorithm. In *2002 International Conference on Pattern Recognition*, pages 545–548. IEEE, 2002. 3
- [19] Julian Chibane, Thiemo Alldieck, and Gerard Pons-Moll. Implicit functions in feature space for 3d shape reconstruction and completion. In *Proceedings of the IEEE/CVF conference on computer vision and pattern recognition*, pages 6970–6981, 2020. 13

- [20] Enric Corona, Gerard Pons-Moll, Guillem Alenyà, and Francesc Moreno-Noguer. Learned vertex descent: a new direction for 3d human model fitting. In *Computer Vision–ECCV 2022: 17th European Conference, Tel Aviv, Israel, October 23–27, 2022, Proceedings, Part II*, pages 146–165. Springer, 2022. 2, 3, 4, 5, 7, 13, 17, 18
- [21] Luca Cosmo, Emanuele Rodola, Jonathan Masci, Andrea Torsello, and Michael M Bronstein. Matching deformable objects in clutter. In *2016 Fourth international conference on 3D vision (3DV)*, pages 1–10. IEEE, 2016. 3
- [22] Bailin Deng, Yuxin Yao, Roberto M Dyke, and Juyong Zhang. A survey of non-rigid 3d registration. In *Computer Graphics Forum*, pages 559–589. Wiley Online Library, 2022. 3
- [23] Theo Deprelle, Thibault Groueix, Matthew Fisher, Vladimir Kim, Bryan Russell, and Mathieu Aubry. Learning elementary structures for 3d shape generation and matching. *Advances in Neural Information Processing Systems*, 32, 2019. 3, 7
- [24] Nicolas Donati, Abhishek Sharma, and Maks Ovsjanikov. Deep geometric functional maps: Robust feature learning for shape correspondence. In *Proceedings of the IEEE/CVF Conference on Computer Vision and Pattern Recognition*, pages 8592–8601, 2020. 7
- [25] Haiwen Feng, Peter Kulits, Shichen Liu, Michael J. Black, and Victoria Fernandez Abrevaya. Generalizing neural human fitting to unseen poses with articulated SE(3) equivariance. In *Proc. International Conference on Computer Vision (ICCV)*, 2023. 3
- [26] Jun Gao, Wenzheng Chen, Tommy Xiang, Alec Jacobson, Morgan McGuire, and Sanja Fidler. Learning deformable tetrahedral meshes for 3d reconstruction. *Advances In Neural Information Processing Systems*, 33:9936–9947, 2020. 5, 14
- [27] Natasha Gelfand, Leslie Ikemoto, Szymon Rusinkiewicz, and Marc Levoy. Geometrically stable sampling for the icp algorithm. In *Fourth International Conference on 3-D Digital Imaging and Modeling, 2003. 3DIM 2003. Proceedings.*, pages 260–267. IEEE, 2003. 4
- [28] Thibault Groueix, Matthew Fisher, Vladimir G Kim, Bryan C Russell, and Mathieu Aubry. 3d-coded: 3d correspondences by deep deformation. In *Proceedings of the european conference on computer vision (ECCV)*, pages 230–246, 2018. 3, 5, 7
- [29] Nikolas Hesse, Sergi Pujades, Javier Romero, Michael J Black, Christoph Bodensteiner, Michael Arens, Ulrich G Hofmann, Uta Tacke, Mijna Hadders-Algra, Raphael Weinberger, et al. Learning an infant body model from rgb-d data for accurate full body motion analysis. In *Medical Image Computing and Computer Assisted Intervention–MICCAI 2018: 21st International Conference, Granada, Spain, September 16-20, 2018, Proceedings, Part I*, pages 792–800. Springer, 2018. 3
- [30] Osamu Hirose. A bayesian formulation of coherent point drift. *IEEE transactions on pattern analysis and machine intelligence*, 43(7):2269–2286, 2020. 3
- [31] Osamu Hirose. Geodesic-based bayesian coherent point drift. *IEEE Transactions on Pattern Analysis and Machine Intelligence*, 2022. 3
- [32] Jiahui Huang, Tolga Birdal, Zan Gojcic, Leonidas J Guibas, and Shi-Min Hu. Multiway non-rigid point cloud registration via learned functional map synchronization. *IEEE Transactions on Pattern Analysis and Machine Intelligence*, 2022. 3
- [33] Ruqi Huang, Jing Ren, Peter Wonka, and Maks Ovsjanikov. Consistent zoomout: Efficient spectral map synchronization. In *Computer Graphics Forum*, pages 265–278. Wiley Online Library, 2020. 3
- [34] Shengyu Huang, Zan Gojcic, Mikhail Usvyatsov, and Konrad Schindler Andreas Wieser. Predator: Registration of 3d point clouds with low overlap. In *IEEE Conference on Computer Vision and Pattern Recognition, CVPR*, 2021. 7
- [35] Puhua Jiang, Mingze Sun, and Ruqi Huang. Neural intrinsic embedding for non-rigid point cloud matching. In *Proceedings of the IEEE/CVF Conference on Computer Vision and Pattern Recognition*, pages 21835–21845, 2023. 3
- [36] Hyomin Kim, Jungeon Kim, Jaewon Kam, Jaesik Park, and Seungyong Lee. Deep virtual markers for articulated 3d shapes. In *Proceedings of the IEEE/CVF International Conference on Computer Vision*, pages 11615–11625, 2021. 3, 7
- [37] Vladimir G Kim, Yaron Lipman, and Thomas Funkhouser. Blended intrinsic maps. *ACM transactions on graphics (TOG)*, 30(4):1–12, 2011. 6, 14
- [38] Diederik P Kingma and Jimmy Ba. Adam: A method for stochastic optimization. *arXiv preprint arXiv:1412.6980*, 2014. 13, 14
- [39] Hao Li, Robert W Sumner, and Mark Pauly. Global correspondence optimization for non-rigid registration of depth scans. In *Computer graphics forum*, pages 1421–1430. Wiley Online Library, 2008. 2, 3
- [40] Jialian Li, Jingyi Zhang, Zhiyong Wang, Siqi Shen, Chenglu Wen, Yuexin Ma, Lan Xu, Jingyi Yu, and Cheng Wang. Lidarcap: Long-range marker-less 3d human motion capture with lidar point clouds. In *Proceedings of the IEEE/CVF Conference on Computer Vision and Pattern Recognition (CVPR)*, pages 20502–20512, 2022. 3
- [41] Tianye Li, Timo Bolkart, Michael J. Black, Hao Li, and Javier Romero. Learning a model of facial shape and expression from 4D scans. *ACM Transactions on Graphics, (Proc. SIGGRAPH Asia)*, 36(6):194:1–194:17, 2017. 2
- [42] Tianye Li, Timo Bolkart, Michael J Black, Hao Li, and Javier Romero. Learning a model of facial shape and expression from 4d scans. *ACM Trans. Graph.*, 36(6):194–1, 2017. 2
- [43] Rong Liu and Hao Zhang. Segmentation of 3d meshes through spectral clustering. In *12th Pacific Conference on Computer Graphics and Applications, 2004. PG 2004. Proceedings.*, pages 298–305. IEEE, 2004. 5
- [44] Matthew Loper, Naureen Mahmood, Javier Romero, Gerard Pons-Moll, and Michael J Black. Smpl: A skinned multi-person linear model. *ACM transactions on graphics (TOG)*, 34(6):1–16, 2015. 2
- [45] Luma AI. Luma ai. <https://lumalabs.ai/>. Accessed: 2023-09-28. 2, 6, 7, 8, 19

- [46] Qianli Ma, Jinlong Yang, Anurag Ranjan, Sergi Pujades, Gerard Pons-Moll, Siyu Tang, and Michael J Black. Learning to dress 3d people in generative clothing. In *Proceedings of the IEEE/CVF Conference on Computer Vision and Pattern Recognition*, pages 6469–6478, 2020. 3, 6, 17
- [47] Naureen Mahmood, Nima Ghorbani, Nikolaus F Troje, Gerard Pons-Moll, and Michael J Black. Amass: Archive of motion capture as surface shapes. In *Proceedings of the IEEE/CVF international conference on computer vision*, pages 5442–5451, 2019. 2, 6, 14
- [48] Riccardo Marin, Simone Melzi, Emanuele Rodolà, and Umberto Castellani. High-resolution augmentation for automatic template-based matching of human models. In *2019 International Conference on 3D Vision (3DV)*, pages 230–239. IEEE, 2019. 3, 5
- [49] Riccardo Marin, Simone Melzi, Emanuele Rodola, and Umberto Castellani. Farm: Functional automatic registration method for 3d human bodies. In *Computer Graphics Forum*, pages 160–173. Wiley Online Library, 2020. 2, 3, 5
- [50] Riccardo Marin, Marie-Julie Rakotosaona, Simone Melzi, and Maks Ovsjanikov. Correspondence learning via linearly-invariant embedding. *Advances in Neural Information Processing Systems*, 33:1608–1620, 2020. 3, 6, 7
- [51] Riccardo Marin, Souhaib Attaiki, Simone Melzi, Emanuele Rodolà, and Maks Ovsjanikov. Smoothness and effective regularizations in learned embeddings for shape matching. *arXiv*, 2023. 3
- [52] Simone Melzi, Riccardo Marin, Emanuele Rodola, Umberto Castellani, Jing Ren, Adrien Poulencard, Peter Wonka, and Maks Ovsjanikov. Shrec 2019: Matching humans with different connectivity. In *Eurographics Workshop on 3D Object Retrieval*, page 3. The Eurographics Association, 2019. 6, 7
- [53] Simone Melzi, Jing Ren, Emanuele Rodola, Abhishek Sharma, Peter Wonka, and Maks Ovsjanikov. Zoomout: Spectral upsampling for efficient shape correspondence. *arXiv preprint arXiv:1904.07865*, 2019. 2, 3
- [54] Simone Melzi, Riccardo Marin, Pietro Musoni, Filippo Bardon, Marco Tarini, and Umberto Castellani. Intrinsic/extrinsic embedding for functional remeshing of 3d shapes. *Computers & Graphics*, 88:1–12, 2020. 3
- [55] Hao Men, Biruk Gebre, and Kishore Pochiraju. Color point cloud registration with 4d icp algorithm. In *2011 IEEE International Conference on Robotics and Automation*, pages 1511–1516. IEEE, 2011. 4
- [56] Ben Mildenhall, Pratul P Srinivasan, Matthew Tancik, Jonathan T Barron, Ravi Ramamoorthi, and Ren Ng. Nerf: Representing scenes as neural radiance fields for view synthesis. *ECCV*, 2020. 7
- [57] Andriy Myronenko and Xubo Song. Point set registration: Coherent point drift. *IEEE transactions on pattern analysis and machine intelligence*, 32(12):2262–2275, 2010. 3
- [58] Vinod Nair and Geoffrey E Hinton. Rectified linear units improve restricted boltzmann machines. In *Proceedings of the 27th international conference on machine learning (ICML-10)*, pages 807–814, 2010. 13
- [59] Dorian Nogneng and Maks Ovsjanikov. Informative descriptor preservation via commutativity for shape matching. In *Computer Graphics Forum*, pages 259–267. Wiley Online Library, 2017. 3
- [60] Maks Ovsjanikov, Mirela Ben-Chen, Justin Solomon, Adrian Butscher, and Leonidas Guibas. Functional maps: a flexible representation of maps between shapes. *ACM Transactions on Graphics (ToG)*, 31(4):1–11, 2012. 2, 3
- [61] Georgios Pavlakos, Vasileios Choutas, Nima Ghorbani, Timo Bolkart, Ahmed A. A. Osman, Dimitrios Tzionas, and Michael J. Black. Expressive body capture: 3d hands, face, and body from a single image. In *Proceedings IEEE Conf. on Computer Vision and Pattern Recognition (CVPR)*, 2019. 5, 13
- [62] Jing Ren, Adrien Poulencard, Peter Wonka, and Maks Ovsjanikov. Continuous and orientation-preserving correspondences via functional maps. *ACM Transactions on Graphics (ToG)*, 37(6):1–16, 2018. 3
- [63] renderpeople. renderpeople. <https://renderpeople.com/>. Accessed: 2023-09-28. 6, 20
- [64] Emanuele Rodolà, Luca Cosmo, Michael M Bronstein, Andrea Torsello, and Daniel Cremers. Partial functional correspondence. In *Computer graphics forum*, pages 222–236. Wiley Online Library, 2017. 3
- [65] Javier Romero, Dimitrios Tzionas, and Michael J Black. Embodied hands: Modeling and capturing hands and bodies together. *ToG*, 2017. 6
- [66] Javier Romero, Dimitrios Tzionas, and Michael J Black. Embodied hands: Modeling and capturing hands and bodies together. *arXiv preprint arXiv:2201.02610*, 2022. 2
- [67] Samuele Salti, Federico Tombari, and Luigi Di Stefano. Shot: Unique signatures of histograms for surface and texture description. *Computer Vision and Image Understanding*, 125:251–264, 2014. 3
- [68] Scan The World Project. Scan the world project. <https://www.myminifactory.com/scantheworld/full-collection>. Accessed: 2023-09-28. 6, 17
- [69] Nicholas Sharp and Keenan Crane. A Laplacian for Non-manifold Triangle Meshes. *Computer Graphics Forum (SGP)*, 39(5), 2020. 5, 14
- [70] Jian Sun, Maks Ovsjanikov, and Leonidas Guibas. A concise and provably informative multi-scale signature based on heat diffusion. In *Computer graphics forum*, pages 1383–1392. Wiley Online Library, 2009. 2, 3
- [71] Ramana Sundararaman, Riccardo Marin, Emanuele Rodolà, and Maks Ovsjanikov. Reduced representation of deformation fields for effective non-rigid shape matching. *arXiv preprint arXiv:2211.14604*, 2022. 3, 7
- [72] Giovanni Trappolini, Luca Cosmo, Luca Moschella, Riccardo Marin, Simone Melzi, and Emanuele Rodolà. Shape registration in the time of transformers. *Advances in Neural Information Processing Systems*, 34:5731–5744, 2021. 3, 5, 7
- [73] Twindom Dataset. Twindom dataset. <https://web.twindom.com/>. Accessed: 2023-09-28. 6, 8
- [74] Lingjing Wang, Jianchun Chen, Xiang Li, and Yi Fang. Non-rigid point set registration networks. *arXiv preprint arXiv:1904.01428*, 2019. 3

- [75] Yue Wang and Justin M Solomon. Deep closest point: Learning representations for point cloud registration. In *Proceedings of the IEEE/CVF international conference on computer vision*, pages 3523–3532, 2019. 3
- [76] Yiheng Xie, Towaki Takikawa, Shunsuke Saito, Or Litany, Shiqin Yan, Numair Khan, Federico Tombari, James Tompkin, Vincent Sitzmann, and Srinath Sridhar. Neural fields in visual computing and beyond. In *Computer Graphics Forum*, pages 641–676. Wiley Online Library, 2022. 4
- [77] Zi Jian Yew and Gim Hee Lee. Rpm-net: Robust point matching using learned features. In *Proceedings of the IEEE/CVF Conference on Computer Vision and Pattern Recognition (CVPR)*, 2020. 4
- [78] Hao Yu, Zheng Qin, Ji Hou, Mahdi Saleh, Dongsheng Li, Benjamin Busam, and Slobodan Ilic. Rotation-invariant transformer for point cloud matching. In *Proceedings of the IEEE/CVF Conference on Computer Vision and Pattern Recognition*, pages 5384–5393, 2023. 3
- [79] Yiming Zeng, Yue Qian, Zhiyu Zhu, Junhui Hou, Hui Yuan, and Ying He. Corrn3d: Unsupervised end-to-end learning of dense correspondence for 3d point clouds. In *IEEE/CVF Conference on Computer Vision and Pattern Recognition (CVPR)*, 2021. 7
- [80] Silvia Zuffi and Michael J Black. The stitched puppet: A graphical model of 3d human shape and pose. In *Proceedings of the IEEE Conference on Computer Vision and Pattern Recognition*, pages 3537–3546, 2015. 3
- [81] Silvia Zuffi, Angjoo Kanazawa, David Jacobs, and Michael J. Black. 3D menagerie: Modeling the 3D shape and pose of animals. In *IEEE Conf. on Computer Vision and Pattern Recognition (CVPR)*, 2017. 2
- [82] Silvia Zuffi, Angjoo Kanazawa, David W. Jacobs, and Michael J. Black. 3d menagerie: Modeling the 3d shape and pose of animals. In *Proceedings of the IEEE Conference on Computer Vision and Pattern Recognition (CVPR)*, 2017. 3

# SUPPLEMENTARY MATERIALS

## Geometric Awareness in Neural Fields for 3D Human Registration

### Abstract

*In this document, we provide further technical details of our method. We also provide an extensive collection of results from the data presented in the paper and a discussion about failure cases, pointing to interesting challenges for future works. We remark here that our method works considering only the point cloud and does not consider the mesh of the target. We show the target mesh only for visualization purposes.*

## 7. Technical details

### 7.1. Implementation details

All the trained NF and Uni- baselines use the same backbone network of [20], which is composed of an IFNet ([19]) to extract global features of the target shape, and an MLP network to query  $\mathbb{R}^3$  points and output offsets (or the universal embedding, in case of Uni- baselines).

**IFNet Network.** We start from a  $64 \times 64 \times 64$  voxelization of the point cloud. Each voxel is represented as the distance from its center to the nearest point of the input. We also compute the discrete gradient of the functions along the three coordinates, and we apply this information to the input. Then, we use twelve 3D Convolutional layers with the following numbers of filters: (64, 64, 128, 128, 192, 192, 256, 256, 256, 256, 256, 256). We assign to each point a set of local and global features considering the output of intermediate layers (one every two) for a total of 1152 features.

**MLPs Query Network.** This network takes the coordinates of a point with the global features extracted by IFNet and predicts all the displacements towards 690 locations, which are the ground truth registered template vertices. In the proposed LoVD, we divided this network into 16 MLPs, each one composed of 6 layers of dimensions (256, 512, 512, 512, 512,  $n$ ) where  $n$  is the number of template vertices belonging to that local part. The local region is obtained by performing spectral clustering on the template described in the next paragraph. The activation function for the first five layers is the ReLu ([58]).

**Training.** The backbone network has in total 36776428 parameters, and it is trained end-to-end. We use a batch size of 8, a learning rate of  $1e - 4$ , and an Adam optimizer ([38]). During training, for each training sample, we query 2200 points: 400 uniformly sampled in  $\mathbb{R}^3$ , and 1800 near the input point cloud, by perturbing the points with random Gaussian noise of standard-deviation 0.05. Hence, the network predicts for each of the 2200 points the offsets towards the ground truth template vertices positions. Before computing the loss, we rescale the offsets with a maximum norm of 0.05, so the network learns to converge in small steps.

### 7.2. INLoVD Details

**INT iterations** For each iteration of our procedure, we consider the vertices of the target point cloud, pass them toward the query network, compute the loss described in Equation 5 of the paper, and backpropagate it to update the weights of the backbone network. This is done for 20 steps using a learning rate of  $1e - 5$  and an Adam optimizer [38]. If the input point cloud is particularly dense, we sample 20000 random points at each iteration.

**Neural Fields Evaluation.** To evaluate the NF, we initialize 690 points at (0, 0, 0) coordinates, and we update their positions 50 times. For the OneShot baseline, we initialize 690 points near the target surface and update their position once. After this, we fit a full 6890 SMPL model to the predicted points, optimizing its parameters for 2000 steps and a learning rate of  $1e - 1$ , using an Adam optimizer ([38]). The loss is a standard L1, plus the statistical pose prior to [61] (weighted for  $1e - 8$ ) and an L2 regularization on the shape parameters magnitude (weighted for  $1e - 2$ ).

**Chamfer Refinement.** The Chamfer refinement optimizes the SMPL parameters using the bidirectional Chamfer Distance between the obtained SMPL and the target point cloud. We perform 500 iterations, with a learning rate of  $2e - 2$  using an Adam optimizer ([38]). We generally considered the bidirectional Chamfer loss when the input point cloud is a complete human model. Otherwise, we optimize only for one direction. We keep the regularizers' weights similar to the previous step.

**SMPL+D.** If the shape contains details that the SMPL model cannot express, we compute the displacements  $\mathbf{O} \in \mathbb{R}^{6890 \times 3}$  to fit the target point cloud. To do so, for each of the SMPL vertices, we optimize the bidirectional Chamfer distance, plus an L2 regularization on the offsets magnitudes and a Laplacian regularization as designed in [26]:

$$L_{lap} = \frac{1}{6890} \sum_{i=1}^{6890} (\Delta(\mathbf{v}_i + \mathbf{O}_i) - \Delta\mathbf{v}_i)^2, \quad (7)$$

Where  $\mathbf{v}_i$  the  $i$ -th vertex the SMPL template resulting from the previous step, and  $\Delta$  the Laplace-Beltrami Operator (in our case, obtained using the Robust Laplacian Python library [69]). This loss promotes the offsets to preserve the smoothness of the input surface. We rely on an Adam optimizer ([38]).

## 8. Further Validations and Ablations

### 8.1. Number of segments.

We trained our backbone network considering different number of segments: 1 (standard LVD), 10, 16, and 24. In all cases, we resized the query MLPs such that they have a comparable number of parameters. Table 6 reports evaluation results. The localization produces a significant gain, while its excess causes performance degradation. Given that using 10 or 16 segments performs similarly, we opted for 16 since it performs better on real scans.

### 8.2. INLoVD Ablation.

To validate the contribution of our registration method, we report in Table 7 the quantitative results after enabling different components. We appreciate the significant improvement provided by INT procedure, upgrading LoVD prediction by a margin of 18% on real scans. To highlight the nature of the contribution, we report in Figure 7 a visualization of the normalized error following the protocol of [37] (*i.e.*, error on X-Axis, percentage of correspondences below that error on Y-Axis). We emphasize that INT increases the number of correct matches (doubling the points with 0 error), and is more robust (the curve saturates faster). The similar saturation of curves for our approach before and after the refinement suggests that our method provides a good initialization for the convergence of Chamfer, which uses the geometry to align local features. All our contributions obtain strictly superior performance compared to the LVD baseline.

### 8.3. INT Robustness and Generalization

**DFAUST.** To further stress our unsupervised INT procedure, we validate its impact on the real scans of DFAUST [9]. Such scans contain noise, missing geometry due to occlusion, and identities significantly far from the

	FAUST <sub>R</sub>	FAUST <sub>S</sub>
LVD	4.78	3.54
LoVD - 10 segments	<b>4.27</b>	3.13
LoVD - 16 segments	4.35	<b>3.11</b>
LoVD - 24 segments	7.92	5.58

Table 6. Ablation study on the number of local MLPs. Increasing the number of components helps, but an excess is also detrimental. Using 10 and 16 segments lead to a good tradeoff, and our full model relies on the second, which performs better on real data.

	FAUST <sub>R</sub>	FAUST <sub>S</sub>
LVD	4.78	3.54
LoVD ( <b>Ours</b> )	4.35	3.11
LoVD+INT ( <b>Ours</b> )	2.97	2.55
INLoVD ( <b>Ours</b> )	<b>1.76</b>	<b>1.85</b>

Table 7. Ablation results for different elements of our pipeline. INT largely improves the backbone’s results, promoting the refinement’s better convergence.

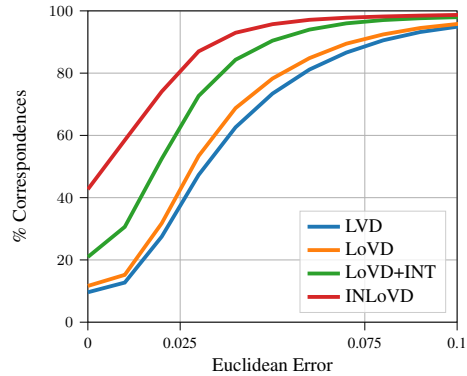


Figure 7. Error curves for ablation study of the pipeline components. We observe that our INT procedure produces a significant impact, doubling the number of exact matches and providing better correspondences.

DFAUST	v2v
INLoVD w/o INT	3.26
INLoVD	<b>3.08</b>

Table 8. Evaluation on 417 DFAUST shapes compared to the ground-truth registration. INT procedure leads to better final registration.

AMASS distribution [47]. We select 11 sequences of different subjects, and we select one frame every ten for a total of 417 scans. We compare INLoVD with and without INT procedure. We evaluate our error using the distance from the provided ground truth registration. We report the results in Table 8. The results confirm that despite the strong initialization provided by the data-driven backbone and the robust SMPL refinement using Chamfer distance, our method provides a further improvement, obtaining a more precise registration. A qualitative comparison is reported in Figure 8.

**Partial Point clouds** INT enables generalization to shapes with geometry significantly far from the training distribution. Here, we show qualitative results of INLoVD when the

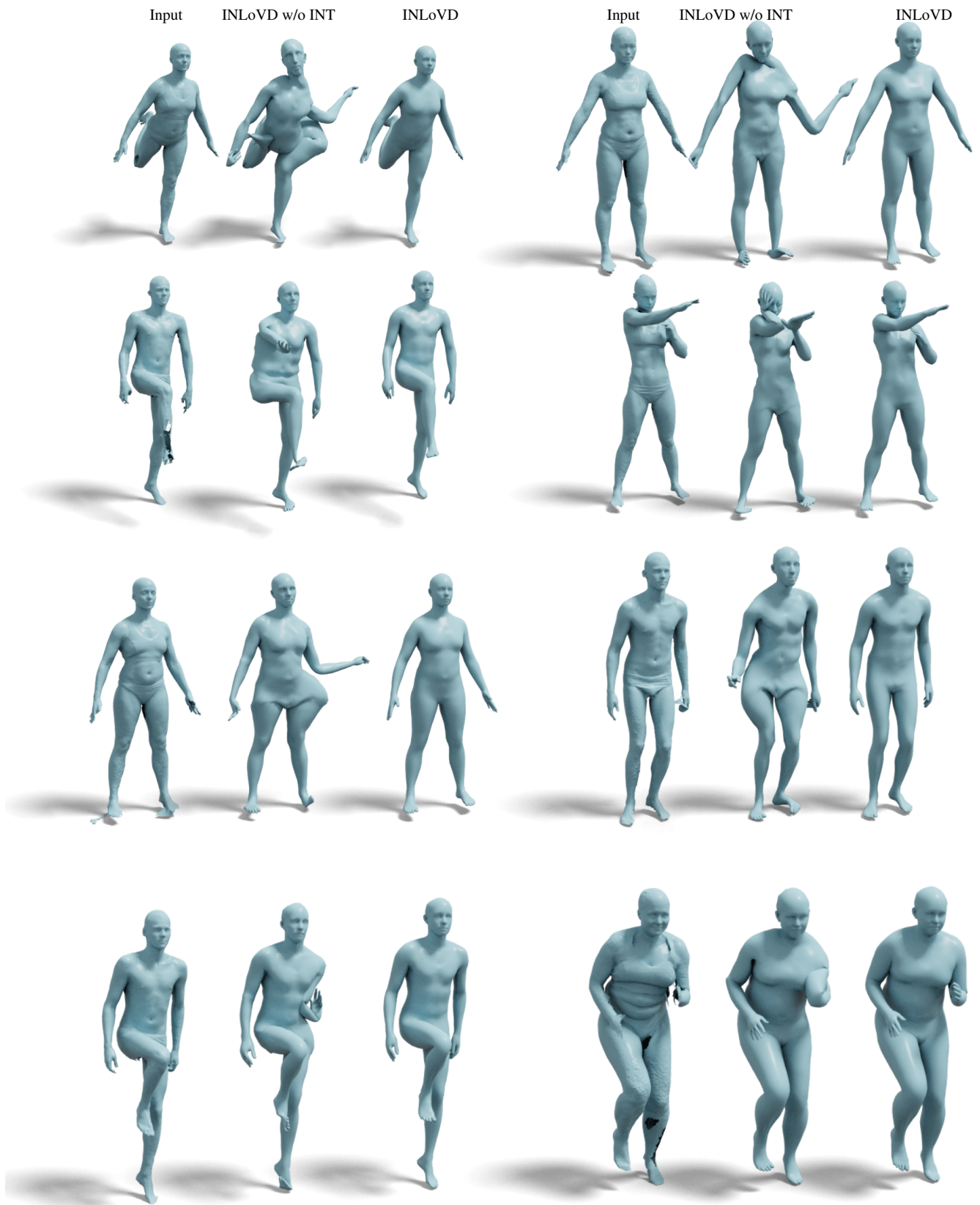


Figure 8. Comparison of results from the full pipeline without and with INT. DFAUST may contain unreferenced vertices, which significantly change the input implicit representation. INT helps to refine these results, bringing the deformation of the backbone towards the majority of points, i.e., the target human.



Figure 9. Comparison of results from INLoVD with and without INT. Partial point clouds are significantly far from the training distribution seen by the backbone network at training time. INT enables this challenging scenario, improving the geometry fitting.

input is a partial point cloud. In Figure 9 we report some results of our method on point cloud coming from DSFN [13] (first two rows) and CAPE [46] (last two rows), with and without INT procedure. INT is crucial and lets the network recover the correct pose of the subject. Without it, the prediction of the backbone is not good enough to initialize the Chamfer refinement, leading to catastrophic failures. We discuss failure cases for our method in the next Section.

**Different Domain and pre-trained networks.** INT runs out of the box on top of any NF. We replicate the experiment on the hands’ registration of [20], using publicly released pre-trained weights and evaluating on the same protocol. We report the errors in Table 9. INT largely improves both vertices and joint estimations. Further qualitative results are reported in Figure 10.

**Non-Humans** Finally, we push the limits of INT in the presence of out-of-distribution proportions and clutter, showing promising results on animals [12] or statues[68] in Figure 11. These can still be represented by a human body template, but only when the template is significantly deformed. To emphasize the contribution of INT refinement, in the same Figure, we also report the result of our pipeline when the procedure is disabled in INLoVD. In these cases, the final output presents significant artifacts, due to a bad initialization of Chamfer refinement that leads to catastrophically local minima.

## 9. Further Results

### 9.1. Failure Cases

During our experiments, we observed some recurrent failure modes for our method. While we show robustness to clutter when it constitutes a significant part of the scene (*e.g.*, large objects), our method cannot distinguish between what is human or not. Our method performs well with disparate identities even significantly far from the training distribution, even on non-humanoids like the ones in Figure 11. Still, when combined with unusual poses, arms and legs might be wrongly located in space. Finally, our method can also recover the human posture in partial point clouds. However, if the input does not contain enough information to define the position of all the human parts, the registration may not find the correct locations for the missing ones attracted by the input point cloud. Examples of these failures are reported in Figure 12, where we can appreciate that some of the body parts are correctly located even in failure cases. We believe that data augmentation combined with segmentation prediction of the input to remove the clutter or highlight what template parts have an image in the input could be a promising direction to address these challenges. Regularizing the INT procedure, considering the initial prediction of the NF could also enhance the procedure’s robustness.

Method	MANO Error		Reconstruction to Scan		Scan to Reconstruction		Target	LVD	LVD+INT (Ours)
	Joint [cm]	Vertex [cm]	V2V [mm]	V2S [mm]	V2V [mm]	V2S [mm]			
LVD	9.6	12.3	5.73	5.73	8.16	6.43			
LVD+INT (Ours)	7.9	10.7	4.73	4.70	6.37	4.15			

Table 9. Hands registration. We apply INT directly to the pre-trained network released by [20]. INT works out of the box and improves all the metrics. On the right is a qualitative comparison.

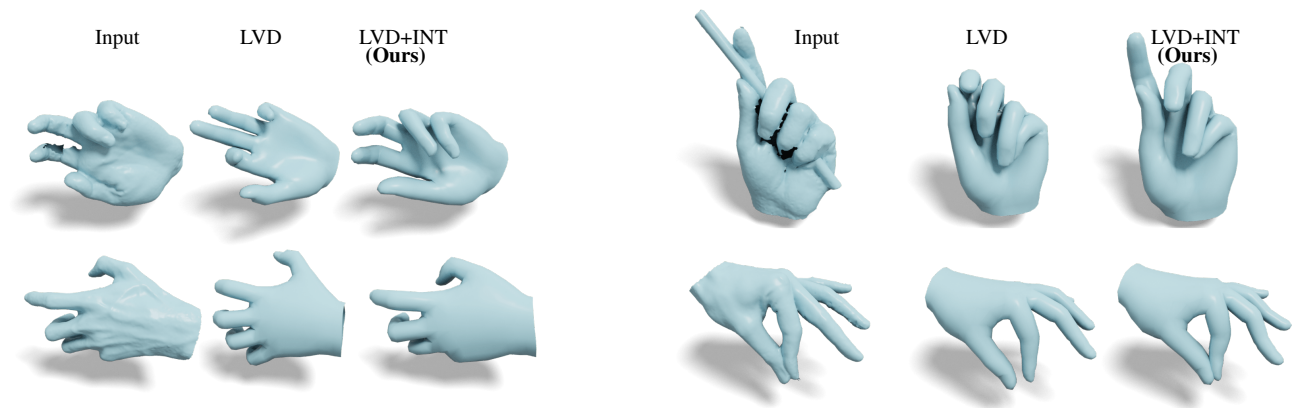


Figure 10. Further results on hand fitting.

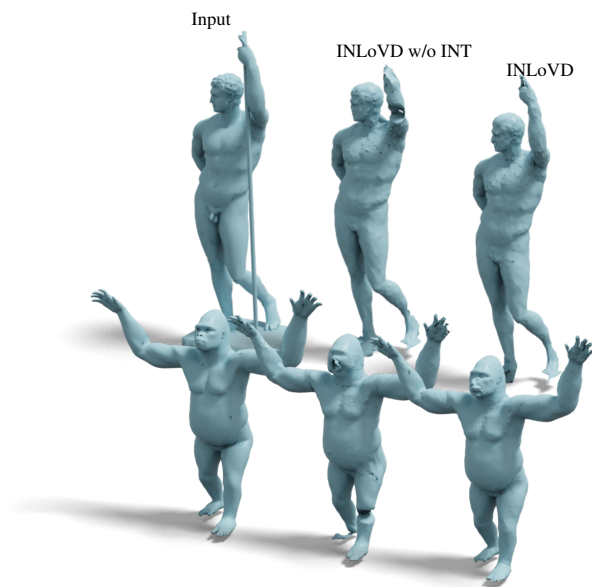


Figure 11. Some results on non-humans models. INT opens to promising generalization results in the presence of highly non-isometries and heavy clutter.

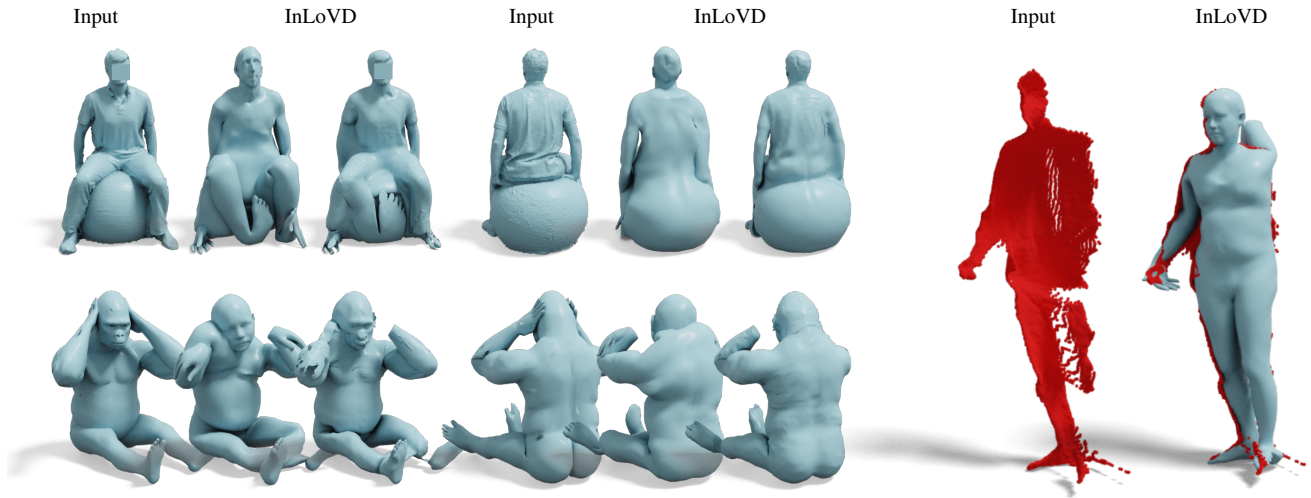


Figure 12. Some failure cases for our pipeline. The presence of heavy clutter, highly unnatural poses, and the complete absence of limbs are among the main failure cases we observed.

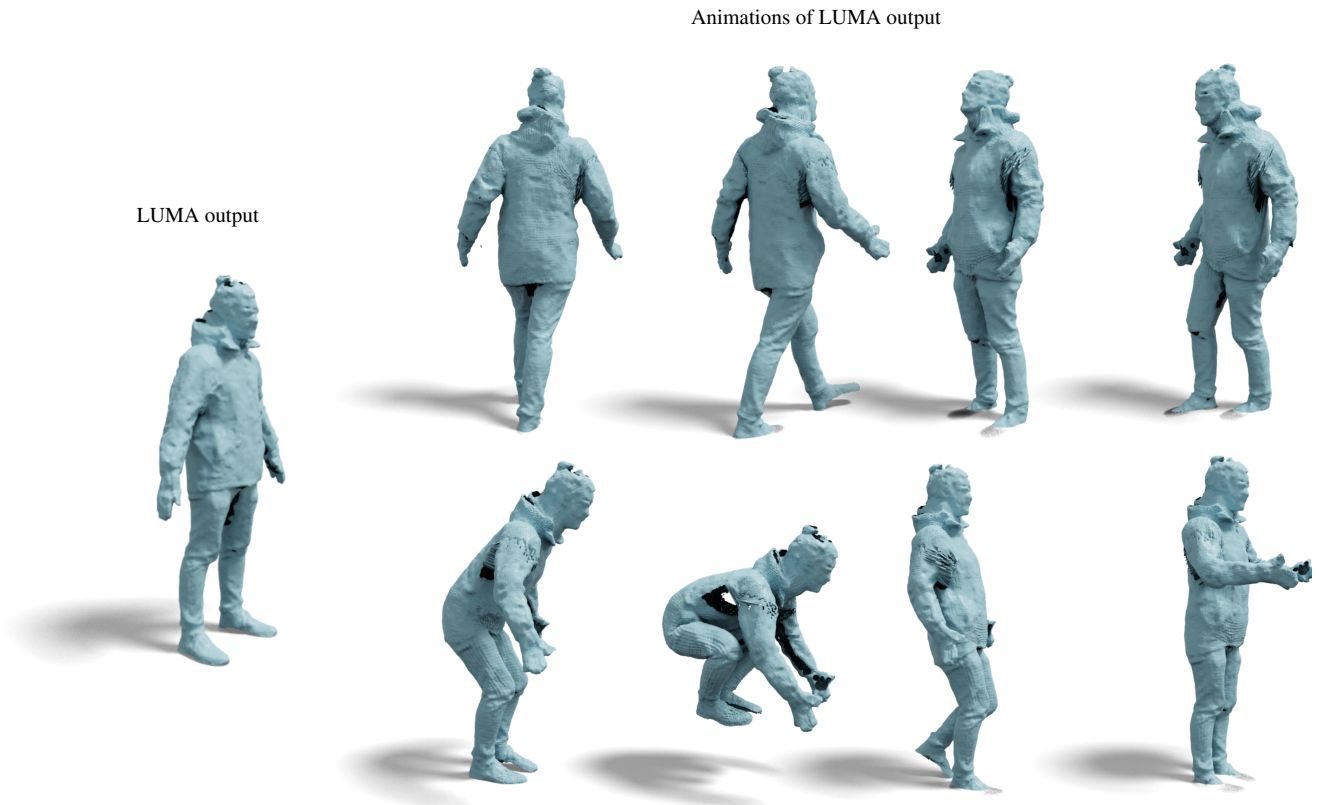


Figure 13. Animatable avatar from [45]. On the left, the geometry was obtained from LUMA. On the right our animation results. Our animation results show semantically coherent motions despite the heavy clothing and gluing that ruined the geometry extracted by LUMA.

## 9.2. Further Qualitative results

**Animation** We show a further example of animation with heavier clothes in Figure 13. Despite the clutter and geometric gluing caused by the garments, our registration is precise enough to provide coherent rigging of the target shape.

**INLoVD results** In the last pages of this document, we show many qualitative results from different datasets. In order:

- Pages 9 to 12: RenderPeople ([63])
- Pages 13 to 17: D-Faust ([9])
- Pages 18 to 21: Test shapes from FAUST challenge ([8])
- Pages 22 to 24: HuMMan ([14])
- Pages 25 to 27: BEHAVE ([14])

For each row, we will display the input and the result of our INLoVD pipeline, both with and without the SMPL+D refinement on the left-hand side. However, for HuMMan and BEHAVE, we will not report the SMPL+D since the shapes in the former do not have significant details, and in the latter, the high-frequency features are primarily noise. It is important to note that we only visualize the meshes for clarity, and our method works solely from the point cloud and does not consider the target mesh in any way. We highlight the variety of poses, clothes, clutter, holes, and identities our method can solve.



# RenderPeople

Input

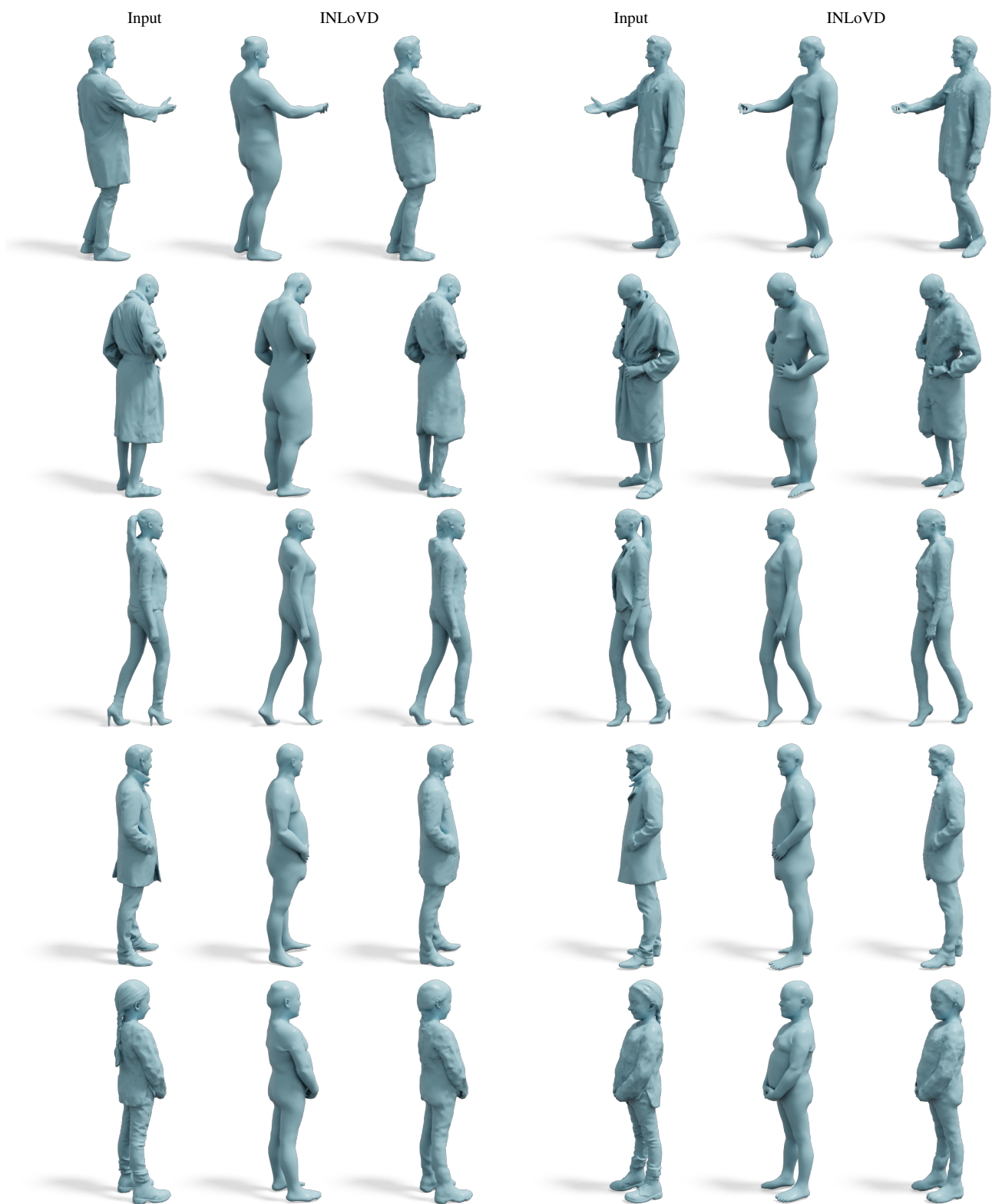
INLoVD

Input

INLoVD



# RenderPeople



# RenderPeople

Input

INLoVD

Input

INLoVD





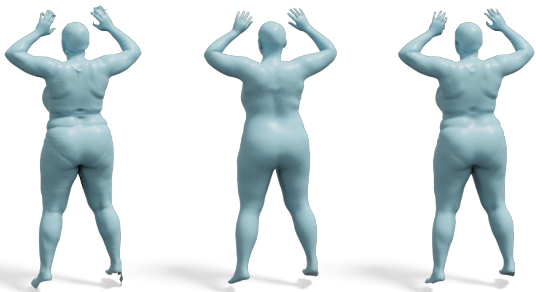
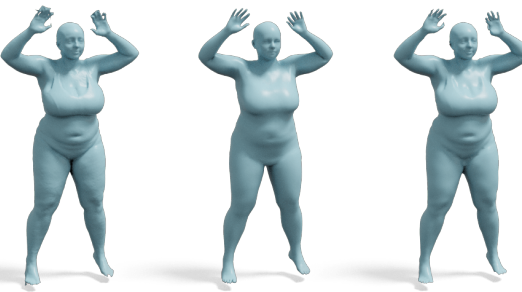
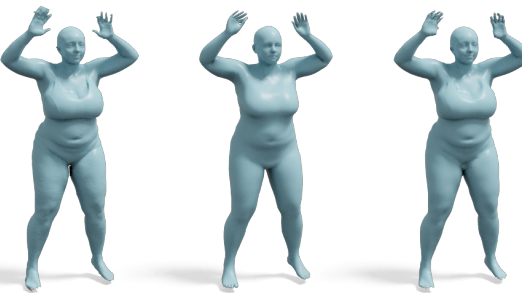
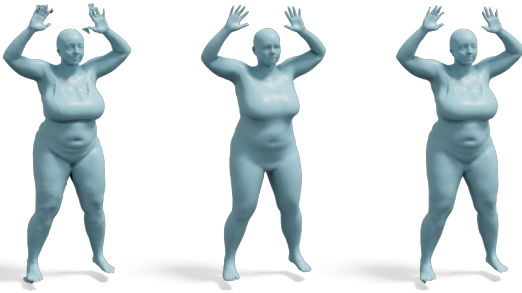
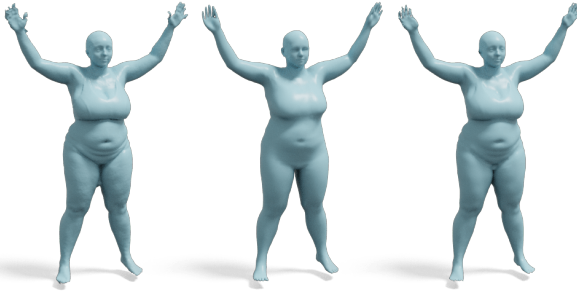
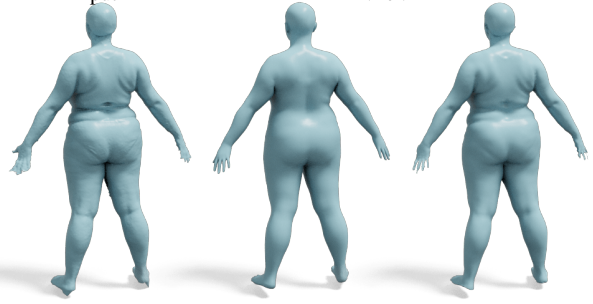
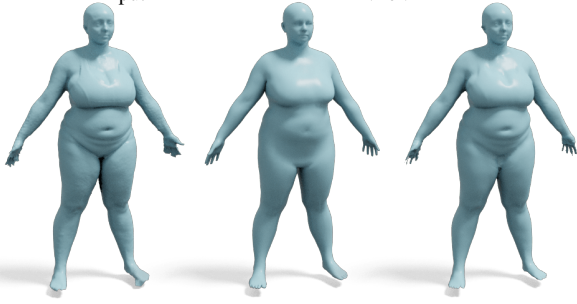
Input

INLoVD

# DFAUST

Input

INLoVD



Input

INLoVD

# DFAUST

Input

INLoVD



Input

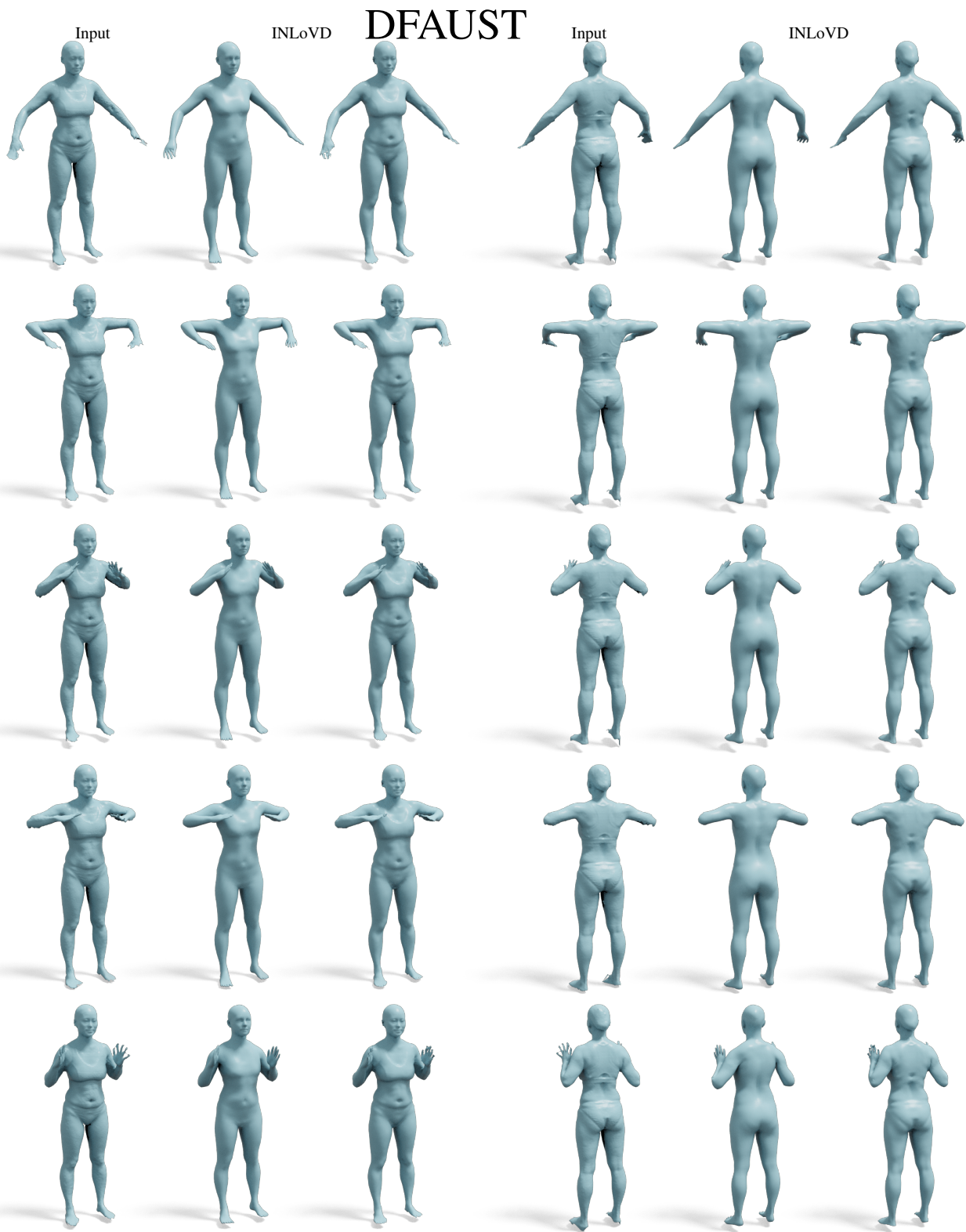
INLoVD

# DFAUST

Input

INLoVD





# FAUST test set

Input

INLoVD

Input

INLoVD



# FAUST test set

Input

INLoVD

Input

INLoVD



# FAUST test set

Input

INLoVD

Input

INLoVD



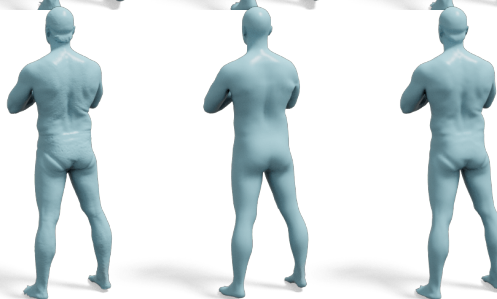
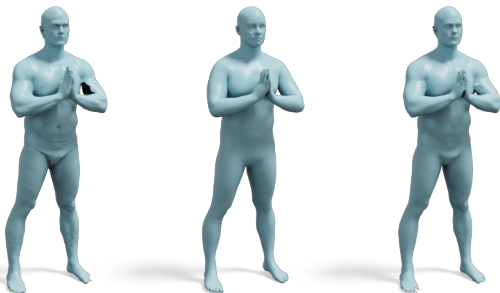
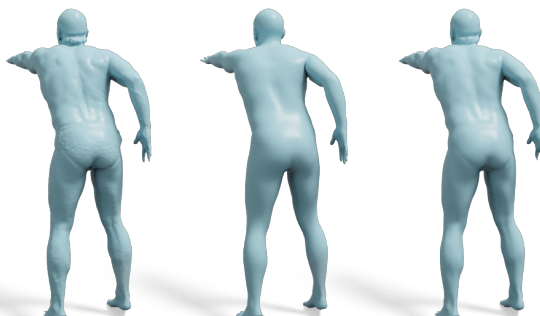
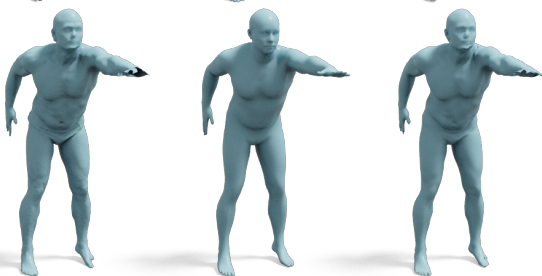
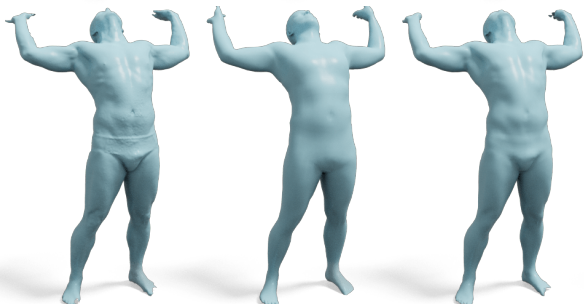
# FAUST test set

Input

INLoVD

Input

INLoVD



Input

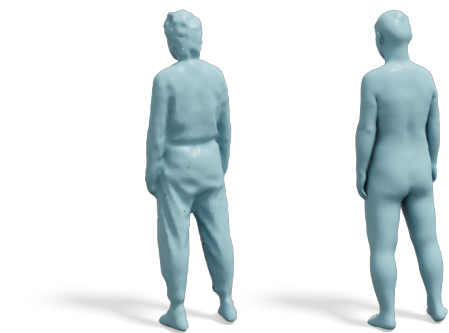
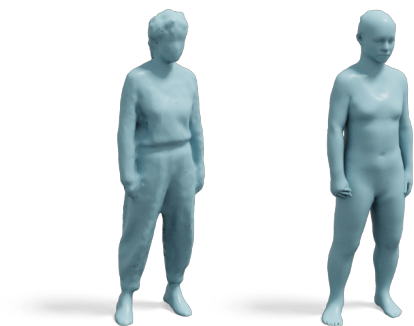
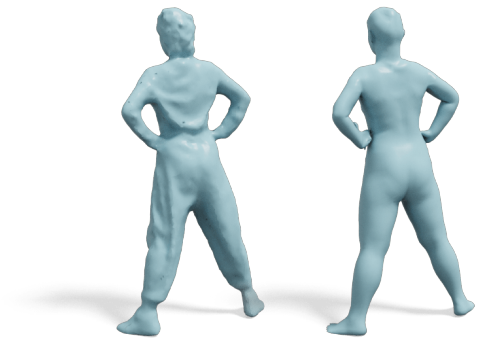
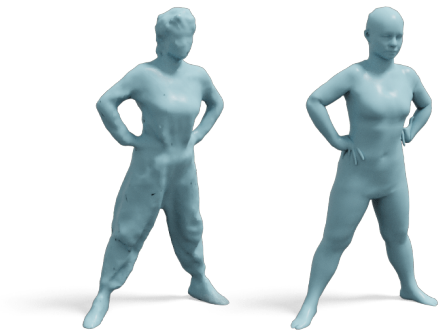
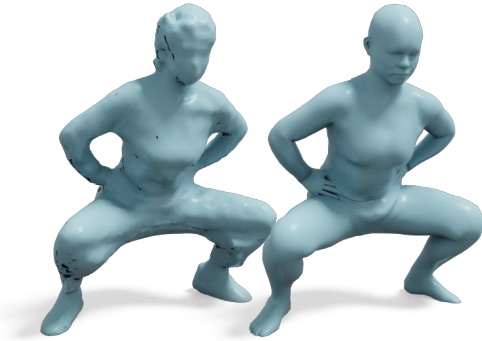
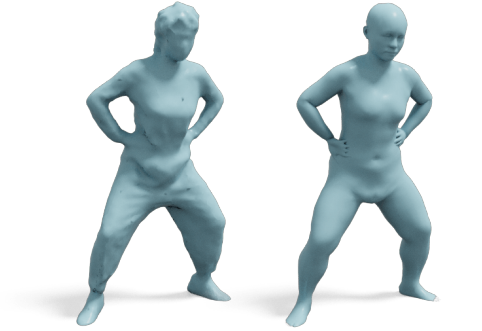
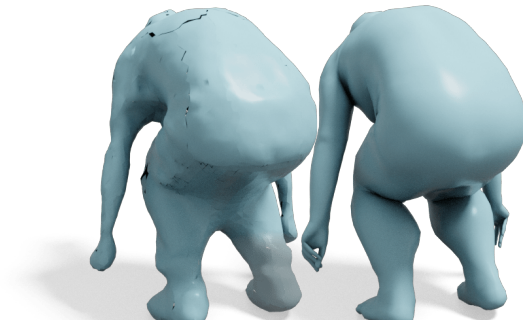
INLoVD

HuMMan



Input

INLoVD



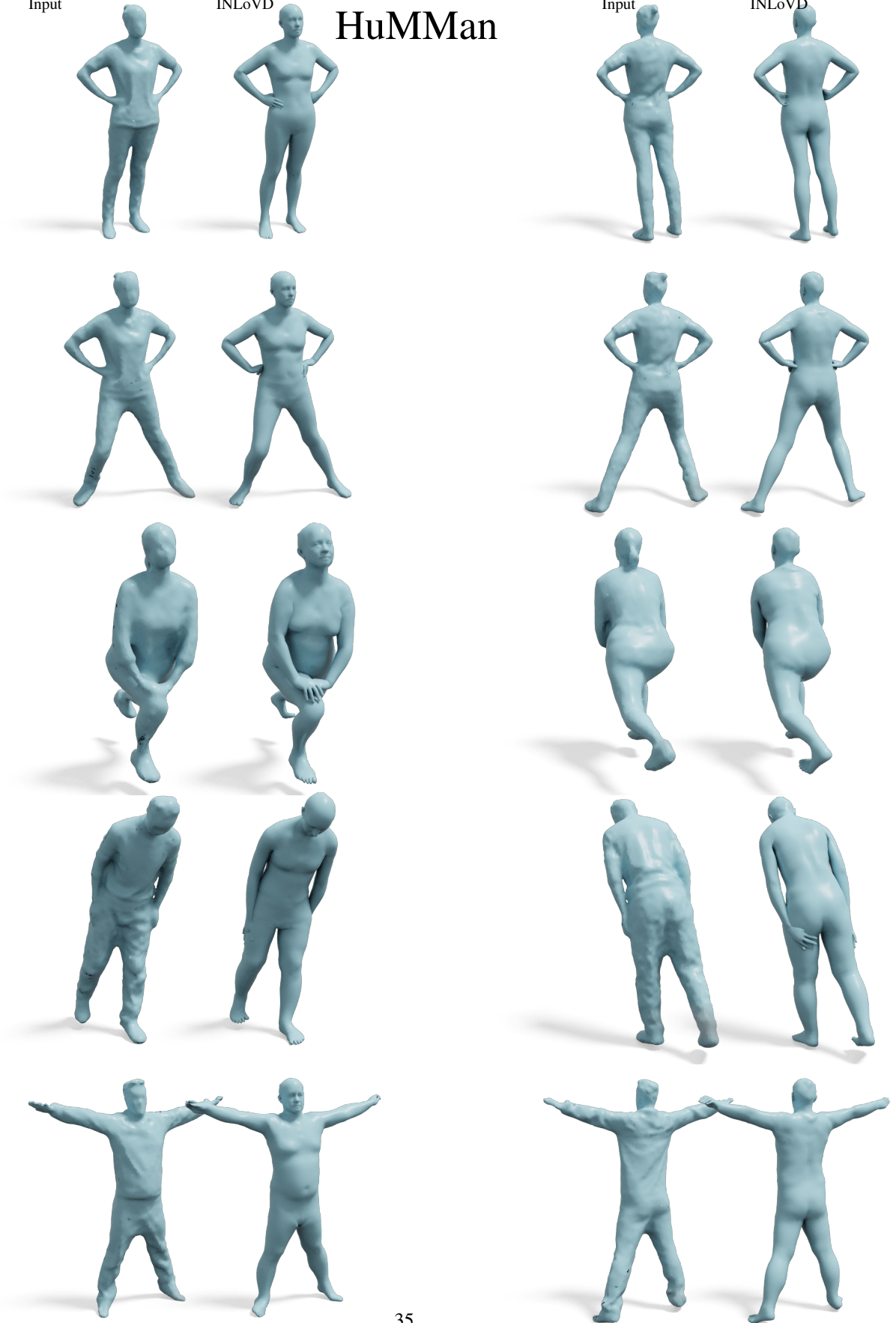
Input

INLoVD

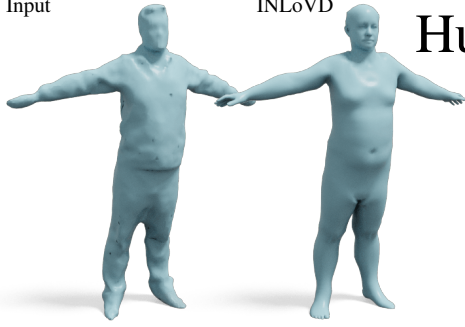
HuMMan

Input

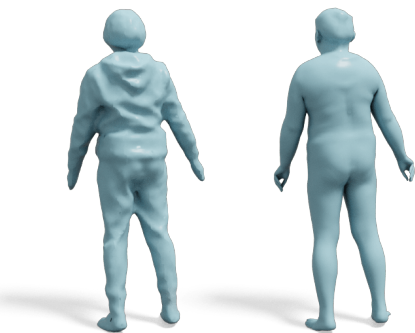
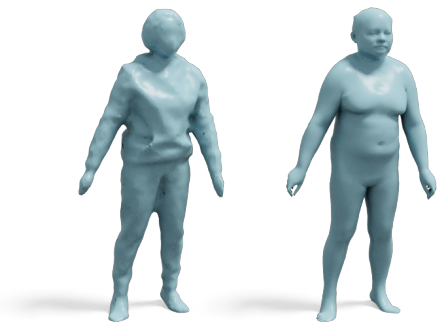
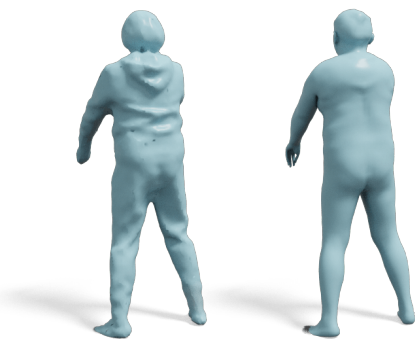
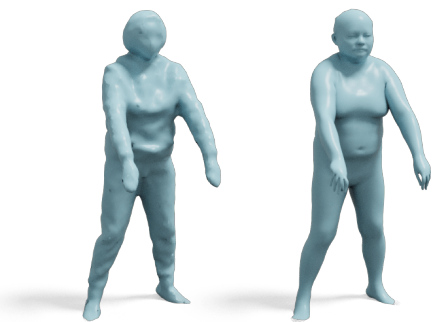
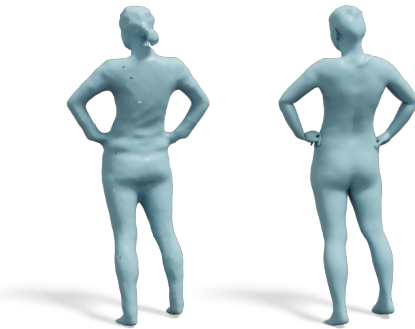
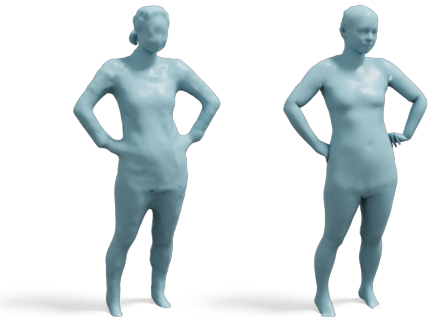
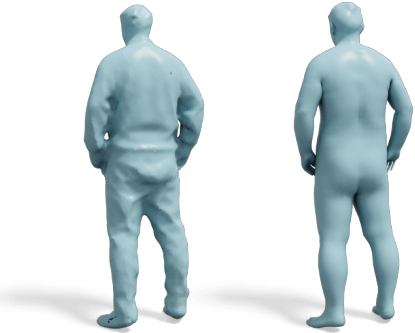
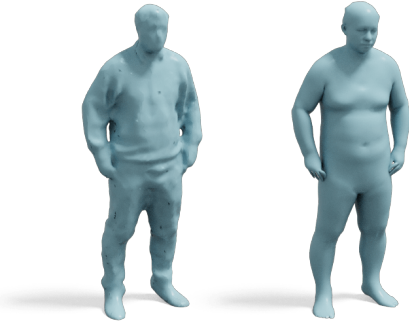
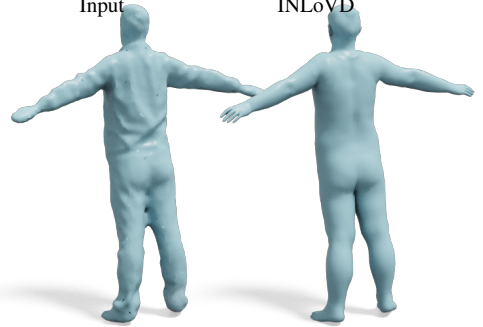
INLoVD



Input INLoVD HuMMan



Input INLoVD



Input

INLoVD

# BEHAVE

Input

INLoVD



# BEHAVE

Input

INLoVD

Input

INLoVD



Input

INLoVD

# BEHAVE

Input

INLoVD

